Adsorption at nanostructured surfaces from first principles

Axel Groß
Institut für Theoretische Chemie, Universität Ulm,
Albert-Einstein-Allee 11, 89069 Ulm/Germany
Email: axel.gross@uni-ulm.de

Nanostructured surfaces often exhibit adsorption properties that are distinctly different from those of flat surfaces. This is the reason for the current interest in the adsorption at nanostructured surfaces, both from the fundamental as well as the applied point of view. In this review, the theoretical modeling and the computational treatment of the interaction of molecules with nanostructured surfaces will be discussed. Since the adsorption of molecules at surfaces involves bond-making and bond-breaking processes, a quantum mechanical description is required which is associated with a relatively large computational effort. Still, because of the progress in the computer power and the development of efficient electronic structure algorithms rather complex molecule-surface systems can be treated from first principles, i.e., without invoking any empirical parameters. The systems addressed in this review include stepped surfaces, supported clusters, surface alloys, nanostructures formed by adsorbate layers, and the dynamics of adsorption on at such a layer. Special emphasis will be put on establishing a microscopic understanding of the specific properties of nanostructured surfaces

Keywords: nanostructures, adsorption, density functional calculations

Contents

1. INTRODUCTION

The interaction of molecules and atoms with surfaces is of strong interest, both from a fundamental as well as from a technological point of view. Materials interact with their environment through their surfaces. They can for example been used to promote chemical reactions, as in heterogeneous catalysis. While these are wanted reactions, there are also unwanted processes such as corrosion and rusting. These processes, on the other hand, can be prohibited by coating and passivating surfaces. Modified properties of substrates due to the interaction of molecules with their surfaces can also been used in sensing.

As far as basic surface science is concerned, the multitude of experimental probes with atomic resolution such as the scanning tunneling microscope (STM)[1] in connection with the ultra-high vacuum technology has allowed a detailed view into the microscopic details of the molecule-surface interaction[2]. Together with the tremendous progress in the computer power and the development of efficient electronic structure algorithms, a very fruitful and close collaboration between theory and experiment for the investigation of the interaction of atoms and molecules with surfaces has become possible[3,4].

However, whereas in the early days of surface science the research was focused on flat low-index surfaces, there is a growing interest in the interaction of atoms and

molecules with nanostructured surfaces. This interest is fueled by the general attention that nanoscience and nanotechnology has received in recent years. Systems with reduced dimensions can exhibit surprising chemical, mechanical, vibrational, electronic, magnetic or optical properties that are distinctly different from those of extended systems. Consequently, also the adsorption properties of molecules can be significantly modified by nanostructuring a substrate.

It is true that surfaces with structures at the nanometer scale have already played a significant technological role for many years, long before the advent of nanotechnology, especially in the field of heterogeneous catalysis. In fact, the activity of many real catalysts is often assumed to be dominated by so-called *active sites*[5], i.e., sites with a specific geometric configuration on the nanometer scale that modifies their electronic and chemical properties. One of the most prominent example is the car exhaust catalyst, where small metal particles on an oxide support are the catalytically active species[6–9]. However, because of the complexity of the systems the exact nature of the catalytically active site is often unknown; and therefore there is still a limited knowledge about the structure-reactivity relationship in heterogeneous catalysis.

In order to develop an understanding about the functional role of nanostructured surfaces in the interaction with molecules it is necessary that well-defined structured surfaces with one particular type of possible active site are studied. One possible way is the preparation of a periodic array of these sites. These can be achieved for example by studying vicinal surfaces where active sites at the steps are separated by supposedly inert terraces of a certain width. One might also create such a periodic array by nanopatterning substrates through adsorbate layers such as organic self-assembled monolayers (SAMs). Another way is the creation of identical nanostructures on surfaces, for example by the deposition of size-selected clusters together with soft-landing techniques resulting in a monodisperse distribution of supported clusters[10].

Because of the still existing complexity in the interaction of molecules with nanostructured surfaces, the interpretation of the experimental results is enormously facilitated if corresponding calculations and numerical simulations are available. The interaction of molecules with surfaces often involve the making and breaking of bonds. Therefore a quantum mechanical theoretical description is required since empirical potentials are usually not reliable enough to properly describe chemical reactions. Fortunately, modern quantum chemical codes based on density functional theory (DFT)[11–14] combine numerical efficiency with a satisfactory reliability and accuracy so that rather complex nanostructures at surfaces can be treated nowadays.

Indeed, a broad variety of surface properties can now be derived from first principles, i.e. without invoking any empirical parameters[15]. First of all, *ab initio* total-energy calculations allow the evaluation of the multi-dimensional potential energy surface (PES) describing the interaction of molecules with surfaces, or at least the determination of special points of the PES such as minima, representing adsorption sites, reaction intermediates and products, or saddle points, representing reaction barriers. However, these calculations offer even more than just total energies. They also yield the electronic structure underlying a particular configuration. The analysis of the electron structure and its interpretation within a conceptual framework can lead to a general understanding of the principles determining the stability of adsorbate structures, chemical trends and the relation between reactivity and structure. In order to achieve an understanding, it is very important to establish reactivity concepts which allow to categorize the immense variety of possible structures and reactions.

It is true that the nanostructures that can be addressed presently by electronic structure calculations are still limited in size. Typically, the nanostructures treated in DFT calculations have dimensions of only 1–3 nm. Nevertheless, it is still possible to extract qualitative trends from theoretical studies, for example as far as the role of low-coordinated sites at the nanostructures is concerned. In addition, the improvement in computer power and the efficiency of the computer codes will make it possible to address larger and larger systems. Furthermore, an efficient computational treatment of the adsorption at nanostructures might involve a multiscale approach on different length scales with the active sites described by a quantum chemical method embedded in a more approximate description of the whole structure.

In this review, I will discuss different types of nanostructured surfaces: stepped surfaces, supported clusters, surface alloys, and nanostructures formed by adsorbate layers. I will not only focus on adsorption geometries but also address reactions at nanostructured surfaces. I will even discuss very recent *ab initio* molecular dynamics simulations at adsorbate-precovered surfaces which are also structured on the nanometer scale. Instead of giving a comprehensive overview over many systems, this review will cover particular well-studied systems which allow to manifest qualitative trends for the interaction of atoms and molecules with nanostructured surfaces.

This review is structured as follows. In the next section, a brief introduction into the theoretical concepts needed for the first-principles description of adsorption on nanostructured surfaces will be given. The third section is devoted to the adsorption on stepped surfaces, while the fourth section covers the adsorption on supported nanoparticles. Then the interaction of molecules with surface alloys will be addressed, followed by a discussion of the nanostructuring of surfaces by adsorbates. The dynamics of the adsorption at nanostructured surfaces will be discussed before finally some conclusions and an outlook will be given where possible directions of further research will be sketched.

2. THEORETICAL CONCEPTS

2.1. Electronic Structure Theory

In the realm of chemistry and solid-state physics, only the kinetic energy and the electrostatic interaction enter the basic expression for the total energy of a physical system. Due to the light mass of the electrons, they have to be treated quantum mechanically. Thus a theoretical analysis "just" requires the solution of the appropriate quantum many-body Schrödinger equation; if heavy atoms are involved so that relativistic effects become important, the relevant equation is the many-body Dirac equation. However, since exact analytical solutions can only be obtained for rather simple systems, numerical methods are required in order to obtain theoretical results.

Wave-function based quantum chemistry methods[16–18] become prohibitively expensive for larger systems because of their unfavorable scaling with the system size. Therefore predominantly electronic structure calculations using density functional theory (DFT)[11,12] are performed in order to address nano-sized systems. They offer a good compromise between computational efficiency and sufficient accuracy for many systems. DFT is based on the Hohenberg-Kohn theorem[11,12] which states that there is a one-to-one correspondence between the electron ground-state density $n(\vec{r})$ and the external potential $V_{\rm ext}$. This means that the exact ground-state density and energy can be determined by the minimization of the energy functional $E[n]$,

$$E_{\rm tot} = \min_{n(\vec{r})} E[n] = \min_{n(\vec{r})}(T[n] + V_{\rm ext}[n] + V_{\rm H}[n] + E_{\rm xc}[n]) \ , \tag{1}$$

where $V_{\rm ext}[n]$ and $V_H[n]$ are the functionals of the external potential and of the classical electrostatic interaction energy, respectively, while $T[n]$ is the kinetic energy functional for non-interacting electrons. These three terms do not contain any quantum mechanical many-body effects which are all lumped together in the so-called *exchange-correlation* functional $E^{\rm xc}[n]$ that is, unfortunately, not known in general. However, it has the important property that it is a well-defined universal functional of the electron density, i.e., it does not depend on any specific system or element.

Instead of using the many-body quantum wave function which depends on $3N$ coordinates now only a function of three coordinates has to be varied. In practice, however, no direct variation of the density is performed, although there is recently a renewed interest in so-called orbital-free DFT calculations[19]. One of the reasons why the formulation (1) is not directly used is that apart from the exchange-correlation functional the kinetic energy functional $T[n]$ is not well-known either.

One rather replaces the many-body Schrödinger equation by a set of coupled effective one-particle equations, the so-called Kohn-Sham equations[12]

$$\left\{ -\frac{\hbar^2}{2m}\nabla^2 + v_{ext}(\vec{r}) + v_{\rm H}(\vec{r}) \ + \ v_{\rm xc}(\vec{r}) \right\} \psi_i(\vec{r}) = \varepsilon_i \, \psi_i(\vec{r}) \ , \tag{2}$$

where $v_{\rm ext}$ is the external potential, the *Hartree potential* $v_{\rm H}$ corresponds to the classical electrostatic potential of the charge distribution $n(\vec{r})$ and the exchange-correlation potential $v_{\rm xc}(\vec{r})$ is the functional derivative of the exchange-correlation functional $E_{\rm xc}[n]$. The electron density $n(\mathbf{r})$ which minimizes the total energy is then given by the sum over single-particle Kohn-Sham states

$$n(\vec{r}) = \sum_{i=1}^{N} \ |\psi_i(\vec{r})|^2 \ . \tag{3}$$

Since the electron density $n(\vec{r})$ that is derived from the solutions of the Kohn-Sham equations (2) already enters the effective one-particle Hamiltonians, the Kohn-Sham equations can only be solved iteratively in a self-consistent field scheme. The ground state energy can then be expressed as

$$E = \sum_{i=1}^{N} \ \varepsilon_i + E_{\rm xc}[n] - \int v_{\rm xc}(\vec{r}) n(\vec{r}) \ d^3\vec{r} - V_{\rm H} \ . \tag{4}$$

Here the first term in the total-energy expression (4) is also called the band structure term $E_{\rm bs}$ since it corresponds to the sum over the single-particle energies.

DFT is in principle an exact theory. However, all the problems associated with quantum mechanical many-body effects are incorporated in the exchange-correlation functional that is not known in general, and hence the reliability of any DFT calculations is directly related to the quality of the chosen approximate functional. For solid-state applications, the so-called local density approximation (LDA) has been astonishingly successful. In the LDA, the exchange-correlation potential of the homogeneous electron gas is used at any position $\vec{r}$ with the corresponding electron density.

However, for chemical binding and reactions at surfaces LDA is not sufficiently accurate[20]. Usually LDA shows *over-binding*, i.e. binding and cohesive energies turn out to be too large compared to experiment. This overbinding also leads to lattice constants and bond lengths that are smaller than the experimental values. These shortcomings of LDA were the reason why many theoretical chemists were rather reluctant to use DFT for a long time. This situation only changed[21] with the advent of exchange-correlation functionals in the Generalized Gradient Approximation (GGA)[22–24]. In the GGA, the gradient of the density is also included in the exchange-correlation energy, but the dependence on the gradient is modified in such a way as to satisfy important electronic sum rules.

Nevertheless, there are also failures associated with the GGA. For example, van der Waals forces are not properly described and band gaps are still underestimated in GGA

by approximately 50%. Furthermore, different GGAs can yield quite varying results, as far as binding and adsorption energies of some molecules are concerned[24]. Still, for many nanostructured systems, the GGA yields a sufficient accuracy, as this review will show.

2.2. Implementation of Electronic Structure Methods

The theoretical modeling of the adsorption on nanostructured surfaces requires the description of at least one hundred atoms on a quantum mechanical level of theory; often the system sizes are even bigger. The most wide-spread methods to deal with systems of this size are DFT codes based on a plane-wave expansion of the Kohn-Sham single-particle states. This is due to the fact that the plane waves are eigenfunctions of the momentum operator so that the kinetic energy can be easily computed in momentum space whereas the potential energy is evaluated in real space, and the switching between real and momentum space is done by efficient Fast-Fourier-Transformation (FFT) techniques.

However, such an approach usually requires a three-dimensional periodicity of the considered system. Hence the molecule-surface systems have to be cast into a three-dimensional periodicity. This is done in the so-called supercell method, in which surfaces are modeled by periodically repeated slabs with a sufficient vacuum layer between them in order to avoid any interaction between the slabs. Figure 1 shows a typical supercell describing the adsorption of atoms at the step sites of a nanostructured fcc(410) surface in a (2×1) geometry. There are two technical parameters that need to be controlled: first, the vacuum layer between the slabs has to be sufficiently wide to avoid any interaction between the slabs, and second, the slabs have to be thick enough to be a reasonable model for a surface of a semi-infinite substrate. Both properties can easily be checked by convergence tests of any calculated property with respect to the width of the vacuum layer and the thickness of the slab. One advantage of the slab approach is that the substrates are infinitely extended in lateral directions which yields a correct description of the delocalized nature of the electronic states of metals, a feature that is not present when the substrates are modeled by finite clusters[25].

On the basis of total-energy calculations, adsorption energies and reaction barrier heights can be determined as the differences of the total energies of the appropriate systems. For example, the *adsorption energy* $E_{\rm ads}$ of a molecule is obtained as

$$E_{\rm ads} \;=\; E_{\rm slab+mol} - (E_{\rm slab} \,+\, E_{\rm mol}) \qquad (5)$$

where $E_{\rm slab+mol}$, $E_{\rm slab}$, and $E_{\rm mol}$ are the total energies per unit cell of the interacting system, the isolated slab, and the isolated molecule, respectively. Using this definition, the exothermic adsorption of molecules is represented by negative energies, as will be done throughout this reveiw. However, sometimes the sign convention is chosen to be the other way around so that one has to be cautious. Here, the absolute value of the adsorption energy will be denoted by the *binding energy*.

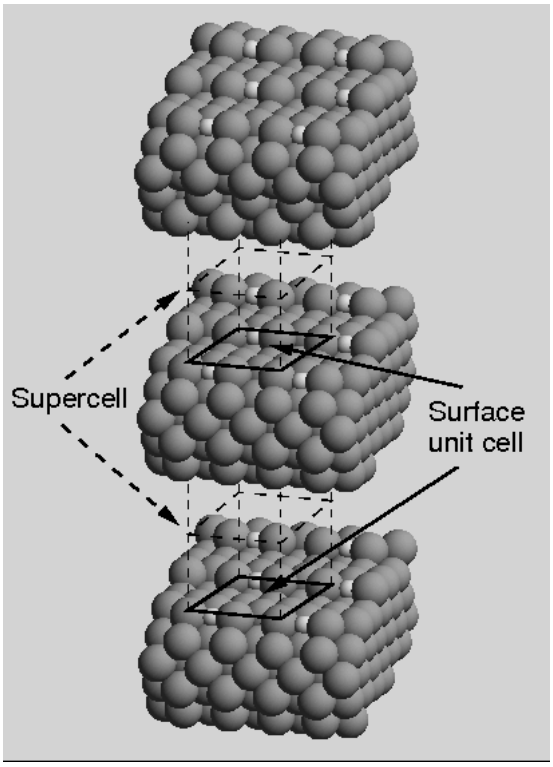

FIG. 1: Illustration of the supercell approach. A substrate of a fcc crystal with a (410) surface termination and an adsorbed periodic atomic layer in a (2×1) geometry is represented by an infinite array of slabs. The supercell and the surface unit cell are indicated in the figure.

In any implementation of DFT, the computational effort is directly linked to the number of electrons that have to be taken into account. Now most chemical and materials properties are governed almost entirely by the valence electrons while the influence of the core electrons on these properties is negligible. This fact is used in the pseudopotential concept[26] in which the influence of the core electrons on the other electrons is represented by an effective potential, the pseudopotential. Since this significantly reduces the number of electrons that have to be taken into account, the use of pseudopotentials leads to an enormous saving of computer time.

A further significant improvement has been the development of *ultra-soft* pseudopotentials[27] and the formulation of the projected augmented-wave (PAW) method[28]. Both methods are indeed closely related[29]. They introduce augmentation charges in the core region in order to create smooth potentials which results in a dramatic reduction in the necessary size of the basis set in plane-wave calculations.

Almost all modern DFT studies presented in this chapter employ the pseudopotential concept, and many large-

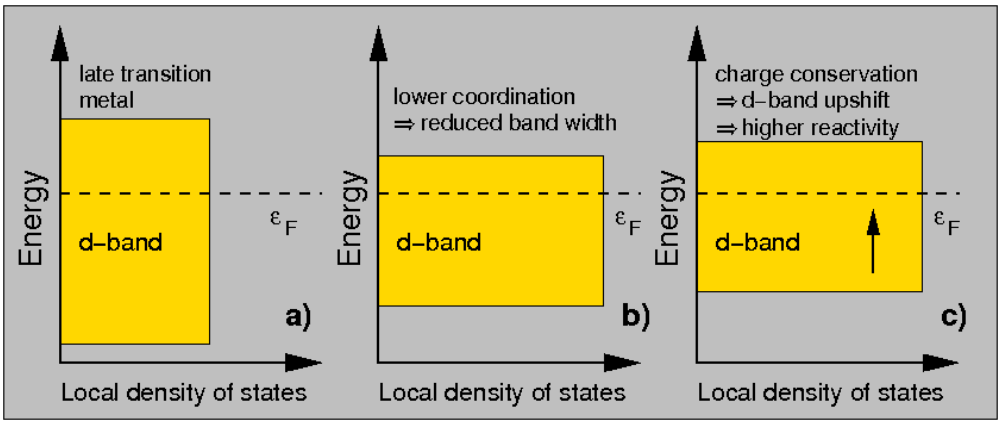

FIG. 2: Illustration of the effect of a lower coordination or smaller atomic overlap on the width and position of a *d*-band. a) *d*-band of a transition metal; b) reduced width of the *d*-band due to a lower coordination or smaller overlap; c) upshift of the *d*-band because of charge conservation.

scale computations would be impossible without the use of pseudopotentials. Using the supercell technique in combination with the pseudopotential or PAW concept, modern efficient DFT algorithms[30–32] can treat up to several hundreds or even thousands of atoms per supercell (see, e.g., [33]).

2.3. Reactivity Concepts

The inspection of total energies alone is usually not sufficient for a deeper understanding of the specific properties of a nanostructured substrate with respect to its interaction with molecules. For this purpose, an analysis of the underlying electronic factors determining the reactivity of the substrate is required, combined with an interpretation of the electronic data within appropriate reactivity concepts.

Fortunately, DFT calculations do not only yield total energies but also information about the electronic structure. It is already rather instructive to examine charge density difference plots, as for example the adsorption-induced charge density difference

$$n_{\rm diff}(\vec{r}) \;=\; n_{\rm total}(\vec{r}) \,-\, n_{\rm adsorbate}(\vec{r}) \,-\, n_{\rm substrate}(\vec{r}) \;. \quad (6)$$

These plots illustrate the charge redistribution and the rehybridization due to the interaction of the reactants. Hence they allow the determination of charge transfer processes, and even the nature and symmetry of the involved orbitals can be deduced from the spatial patterns.

Additional information can be gained from the electronic structure in momentum and energy space, i.e., from the electronic orbitals and bands that are involved in the adsorption process. This information can be deduced from the determination of changes in the local density of states (LDOS) which is defined by

$$n(\vec{r},\varepsilon) \;=\; \sum_i \; |\phi_i(\vec{r})|^2 \; \delta(\varepsilon - \varepsilon_i) \;. \quad (7)$$

There is a rather simple but still very useful reactivity concept, namely the so-called *d*-band model[34,35], that has been very successful in explaining chemical trends in the interaction of molecules with *d*-band metals which are relevant for catalytic applications. This scheme is closely related to the frontier orbital concept developed for gas-phase reactions[36,37]. In the *d*-band model, the whole *d*-band is replaced by an effective level located at the center of the *d*-band ε_d. This level plays the role of the substrate frontier orbitals, i.e. of the highest occupied molecular orbital (HOMO) and the lowest unoccupied molecular orbital (LUMO).

According to the *d*-band model, the reactivity of a substrate is directly related to the energetic position of the *d*-band center ϵ_d. It is particular useful for comparing the reactivity of similar systems. In such a situation the *d*-band model states that there is a linear relationship between the *d*-band center shift $\delta\varepsilon_d$ and the change in the chemisorption strength ΔE_d[38,39],

$$\delta E_d = -\frac{V^2}{|\epsilon_d - \epsilon_a|^2} \; \delta\varepsilon_d \;, \quad (8)$$

where ϵ_a is an electronic adsorbate level and V is a coupling matrix element that is assumed to be constant for similar situations. Eq. (8) means that there is a stronger interaction or larger energy gain upon an upshift of the *d*-band.

This concept provides an intuitive picture for the enhanced reactivity of nanostructured surfaces which is illustrated in Fig. 2. Consider a typical transition metal with a more than half-filled *d*-band (Fig. 2a). At a step atom or at some other low-coordinated site, the local *d*-band density of states will be modified. In a simple tight-binding picture, the width of a band is directly related to the coordination and the overlap of the orbitals. At a low-coordinated site, the *d*-band will therefore become narrower (see Fig. 2b). Note that the same is in fact also true for pseudomorphic overlayers under tensile strain which reduces the overlap between the electronic

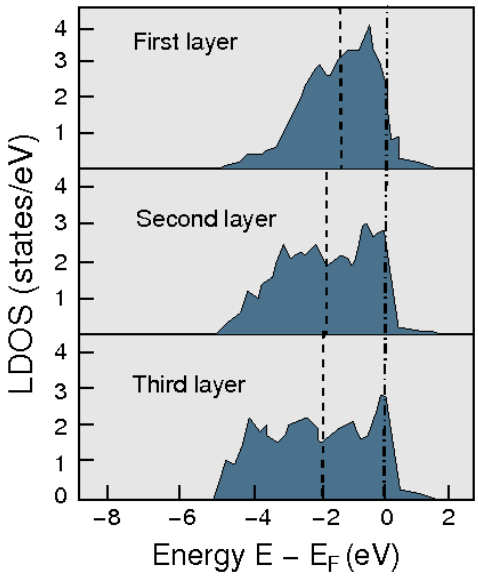

FIG. 3: Layer-resolved, local d-band density of states of Pd(210) determined by GGA-DFT calculations. The Fermi level and the center of the d-band are indicated by vertical dash-dotted and dashed lines, respectively. The third-layer LDOS is already very close to the bulk density of states of palladium (after [45]).

orbitals[40–44]. Now if the d-band is more than half-filled but not completely filled and the d-band center is kept fixed, the number of d-states below the Fermi energy will increase. This would lead to an higher occupation of the d-band. However, the number of d-electrons is conserved. In order to obey charge conservation, the narrower d-band has to shift up (Fig. 2c) so that the number of occupied states remains unchanged. Thus also the d-band center will move up. According to the d-band model, this results in a higher reactivity of the structured system.

The simple concept of the d-band upshift due to the band narrowing is illustrated in Fig. 3, where the layer-resolved d-band LDOS of the stepped Pd(210) surface is plotted according to GGA-DFT calculations[45]. The LDOS of the third layer is almost identical to the Pd bulk density of states. This is a consequence of the good screening properties of metals[46] which lead to a rapid recovery of bulk properties in the vicinity of imperfections such as surfaces. However, the width of the d-band of the second and first layer are significantly reduced compared to the third layer. And this reduction in band width is indeed accompanied by an upshift of the d-band centers, as indicated by the vertical dashed lines. This upshift leads to stronger adsorption at the step sites[45,47], as will be discussed in the next section. Note that the density of states effects are only related to the band-structure energy. This is, however, only one term in the sum yielding the Kohn-Sham total energy. There are many systems where electrostatic effects or even exchange-correlation effects contribute to the chemical reactivity and interaction strengths.

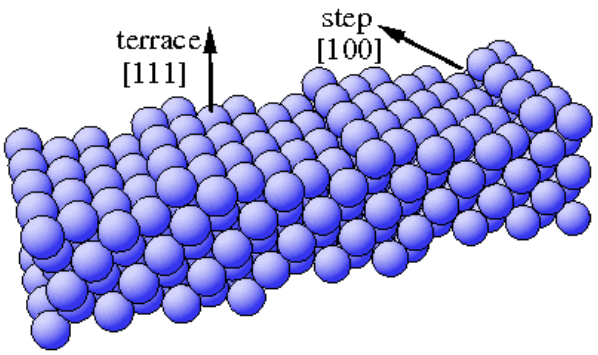

FIG. 4: A stepped (755) = 6(111) × (100) vicinal surface. Steps with ledges of (100) orientations separate (111) terraces that are 6 atom rows wide

3. ADSORPTION ON STEPPED SURFACES

3.1. Vicinal surfaces

Nanostructures at surfaces often exhibit a broad variety of possible adsorption sites because of their open defect-rich structure. This makes a microscopic identification of the relation between the geometric and electronic structure and its reactivity towards adsorption rather complicated. Therefore it is advantageous to study surface structures with one well-defined defect type so that its influence can be isolated from that of all other possible structures.

In particular *vicinal surfaces* allow to assess the influence of steps on, e.g., adsorption properties or reactions on surfaces in a systematic way. These surfaces are only slightly misaligned from a low index plane so that a periodic array of terraces of a low-index orientation separated by monoatomic steps results. They are also well-suited for a combined experimental and theoretical investigation since they can be relatively easily prepared in the experiment and they are accessible to electronic structure calculations.

A typical vicinal surface in illustrated in Fig. 4. The structure shown corresponds to (755) surface which consists of 6 atomic rows of (111) orientation separated by a step with a (100) ledge, i.e., the ledge represents square (100) microfacets. The misalignment from the [111] direction is 9.5°. Vicinal surfaces are often denoted by $n(hkl) \times (h'k'l')$[48] where (hkl) and $(h'k'l')$ are the Miller indices of the terraces and of the ledges, and n gives the width of the terraces in number of atomic rows parallel to the ledges. Thus a (755) surface is represented by $6(111) \times (100)$. Another example is the $(911) = 5(100) \times (111)$ surface that is rotated by 9.5° from the [100] direction.

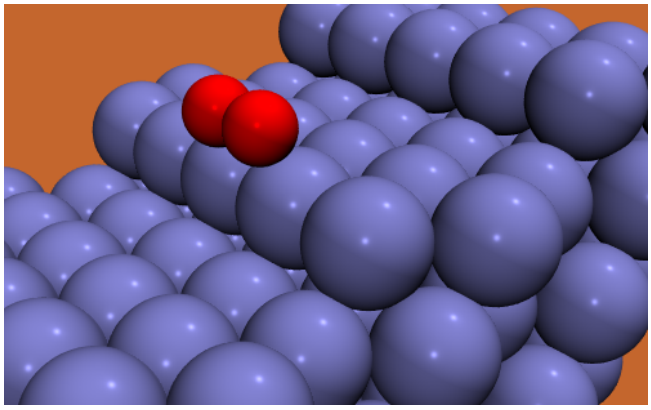

FIG. 5: Molecular O_2 adsorption site at the steps of a Pt(211) surface determined by DFT calculations[50]. For the sake of clarity, the O_2 coverage in the figure does not correspond to the one used in the calculations.

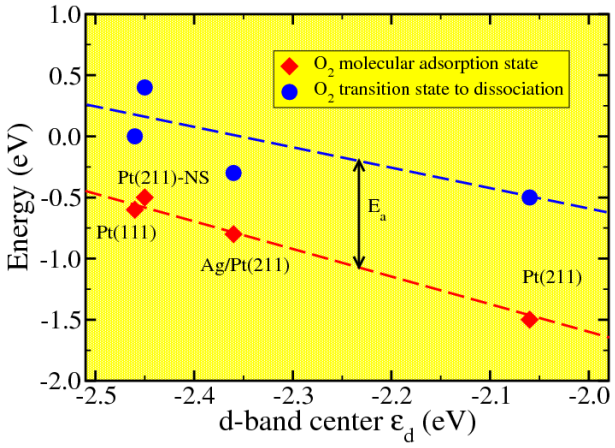

FIG. 6: O_2 molecular adsorption energy and transition state energies determined using the GGA-PW91 functional as a function of the local d-band center ε_d[62]. The dashed lines are included as a guide to the eye.

3.2. Adsorption of simple molecules on stepped metallic surfaces

Experimentally, it is well-known that many adsorbates bind preferentially to step sites[49,50]. This has of course motivated electronic structure calculations. A particularly well-studied system is the adsorption of CO on Pt surfaces. The binding energies of CO at the on-top sites of several flat, stepped, kinked and reconstructed Pt surface have been investigated by DFT-GGA calculations[38]. These calculations have revealed a strong structure sensitivity of the binding strength with variations of 1 eV in the CO adsorption energies.

As far as stepped surfaces are concerned, the Pt(211) and Pt(11 7 5) surfaces have been considered. Both surfaces have (111) terraces of similar width, but while the (11 7 5) surface has a open kinked structure along the steps, the (211) surface is close-packed along the steps (see Fig. 5). And indeed, the lowest-coordinated Pt atoms which are the kink atoms of the (11 7 5) surface show the strongest binding to CO with bonding energies that are about 0.7 eV stronger than on the flat Pt(111) terrace. These findings have again been rationalized using the d-band model[38]. The lower the coordination, the larger the d-band shift and consequently the higher the adsorption energy.

Apart from the CO/Pt system, the interaction of molecular oxygen with Pt surfaces represents one of the best studied systems in surface science, both experimentally[51–56] as well as theoretically[57–61]. This interest, as for CO/Pt, was also motivated by the technological relevance of the adsorption and dissociation of O_2 on Pt as a crucial microscopic reaction step occuring in the car-exhaust catalyst. O_2 can adsorb both molecularly and dissociatively on Pt. In fact, molecular dynamics simulations revealed that because of steric hindrances oxygen always adsorbs molecularly before it dissociates [59,60], even if the molecules impinge on the surface with kinetic energies much larger than the dissociation barrier, in agreement with experiments at low surface temperatures[53].

Experimentally, the influence of steps on adsorption properties can be relatively easily identified since steps can be readily decorated and thus passivated by some inert metal, for example Ag. Thus it was found that the O_2 dissociation is strongly favored at the step sites of Pt[9(111) × (111)] and Pt[8(111) × (100)][50], which have both (111) terraces that are nine and eight atom rows wide, separated by {111} and {100} monatomic steps, respectively. In order to understand the enhanced reactivity of the Pt steps, GGA-DFT calculations were performed[50,62]. In order to reduce the computational effort, the O_2 adsorption and dissociation was studied on Pt(211)=Pt[3(111) × (100)] where the terraces are only three atom rows wide. They are still far enough from each other in order to make the calculations relevant for the understanding of the reactivity of the vicinal surfaces.

In the calculations, the O_2 molecular adsorption state and its energy E_{mol} and the energy of the transition state to dissociation E_{TS} were determined for the step site and a "near step" (NS) site one row away from the steps of the clean Pt(211) surface and for the Pt(211) surface with the steps decorated by a monatomic row of silver atoms. The energetically most favorable molecular adsorption state of O_2 on Pt(211) which is shown in Fig. 5 is indeed at the Pt step atoms. The same is true for oxygen atoms which also preferentially adsorb at the Pt step atoms[63].

The fact that oxygen atoms and molecules bind more strongly to steps can again be understood within the d-band model. In Fig. 6, the energies of the O_2 molecular adsorption state and the transition state to dissociation on Pt(211) are compared to the corresponding ones for the Pt(111) surface as a function of the local d-band center ε_d. There is an obvious correlation between the energies and the position of ε_d. At the step sites, the low

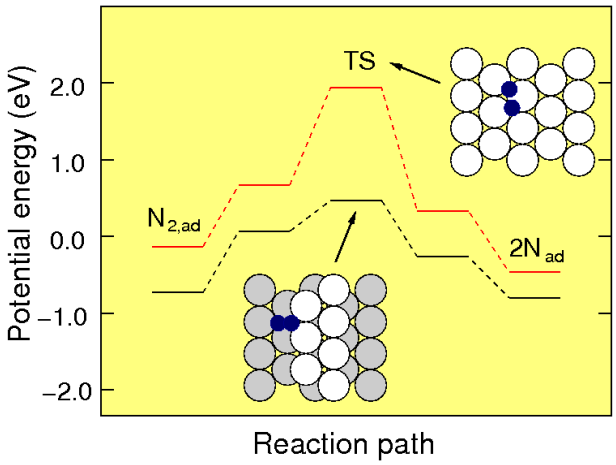

FIG. 7: Energetics of the N_2 dissociation on a terrace and a step of Ru(0001) as determined by DFT calculations[64]. The insets show the corresponding configurations at the transition state (TS) for dissociation. The energy zero is chosen to be the energy of the N_2 molecule in the gas phase.

coordination leads to a upshift of the *d*-band center resulting in a stronger interaction.

Interestingly enough, the local barrier for dissociation $E_a = E_{\rm TS} - E_{\rm mol}$ is not reduced at the steps of Pt(211); on the contrary, it is even higher than on the flat Pt(111) surface. At first sight, it seems to be surprising that there is a higher rate for dissociation at the steps. However, not only the height of the local dissociation barrier matters, but also the absolute energetic position of the transition state with respect to the O_2 molecule in the gas phase. For Pt(111), the transition state energy and the energy of O_2 in the gas phase are almost equal which means that the dissociation barrier and the desorption barrier are similar. Hence, in a thermally activated situation, a large fraction of the molecules will rather desorb than dissociate. This is different at the steps where the transition state energy is well below the O_2 gas phase energy. Hence the desorption barrier is much larger than the dissociation barrier so that the branching ratio between dissociation and desorption is strongly shifted towards dissociation although the absolute value of the barrier is higher at the steps. Consequently, it is the stabilization of the molecular adsorption state that leads to an enhanced dissociation at steps.

However, there are systems such as N_2 dissociation on Ru(0001) where reaction barriers are significantly lowered at step sites, as experiments have shown[64,65]. This system is of particular importance since the N_2 dissociation represents the first and rate-limiting step in the ammonia synthesis[66,67]. The Ru(0001) surface used in the experiments had a step density of less than 1%. By again blocking the step sites with less than 2% of a monolayer of gold it could be shown that at 500 K the dissociation rate at the steps is at least nine orders of magnitude higher than on the terraces[64,65].

The dissociation of N_2 on flat and step Ru(0001) surfaces was addressed by DFT calculations[64,68] in which the step was modeled by using a (2×4) unit cell and removing two rows of Ru atoms. As Fig. 7 demonstrates, the barrier for the dissociative adsorption of N_2 at the steps is significantly lowered from 1.9 eV on the terraces to 0.4 eV at the steps, in qualitative agreement with the experiment. Note that whereas the N_2 molecular precursor is also strongly stabilized at the steps, the difference in the binding energies of atomic nitrogen at the steps and the terraces is much smaller. This is important because it means that the nitrogen atoms do not block the step sites after dissociation but can diffuse towards the terraces.

In order to understand the strongly modified reactivity of the steps, it is instructive to examine the transition state configurations on the terrace and at the step. At first sight, they do not seem to be too different. In both cases, one nitrogen atom is close to the most stable hcp site while the other one is located at a bridge position. However, at the step the two N atoms do not share any Ru atoms as nearest neighbors. This reduces the indirect repulsive interactions which is the reason for the high N_2 dissociation barrier on the terrace[69]. Hence it is the modified geometrical arrangement of the steps that contributes significantly to the higher reactivity.

A dramatic lowering of the dissociation barrier at stepped ruthenium surfaces has also been found for NO. According to DFT calculations, this barrier is reduced from 1.28 eV at the flat Ru(0001) surface to 0.17 eV at a stepped Ru surface[70], thus rationalizing experimental findings of a STM study that NO dissociation only occurs at the steps of a vicinal Ru surface[71]. A closer analysis yields that this strong reduction is caused by so-called final state effects. First, the reaction products, atomic nitrogen and oxygen are more strongly bound at the steps than on the terrace, and second, at the steps the reaction products share less nearest neighbor surface atoms, as in the case of N_2 dissociation. This confirms that the modified structural arrangement at the steps plays a very important role for the reactivity.

The specific structural arrangement at steps can also induce unusual adsorbate structures. Hydrogen molecules usually do not adsorb molecularly on metal surfaces, but rather dissociatively[72]. Molecularly chemisorbed H_2 species have only been found at stepped metal surfaces. On Ni(510), a molecular adsorption state at surface temperatures up to 125 K has been observed at the step sites, but only after the surface was passivated with a dense atomic hydrogen layer[73]. On Cu(510), a weakly bound species has been observed at low temperatures on the clean surface[74,75].

The hydrogen/palladium system has been a model system for the study of the interaction of hydrogen with metal surfaces[76–78]. The interest in the system was in part motivated by the potential role of palladium as a hydrogen storage material. DFT calculations confirmed the experimental findings that hydrogen adsorbs only dissociatively on low-index Pd surfaces[79–81]. However, on

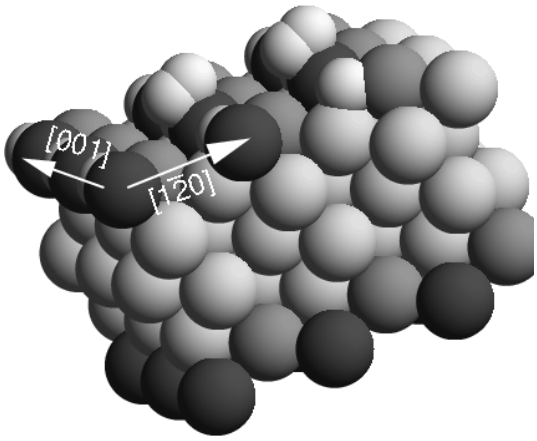

FIG. 8: Structure of the Pd(210) surface together with adsorbed hydrogen atoms at the open (110)-like microfacets and two adsorbed hydrogen molecules[45,47].

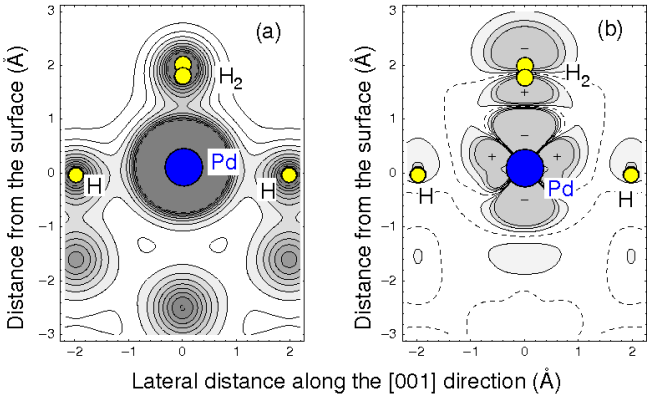

FIG. 9: Electron density plots of the molecular adsorption state in the plane spanned by the surface normal and the direction along the steps. The positions of the H atoms and the top Pd atom are marked by open (yellow) and filled (blue) circles, respectively. a) Total charge density, b) charge density difference[45,47].

the stepped Pd(210) surface, isotope exchange experiments indicated the coexistence of chemisorbed hydrogen atoms and molecules[47]. The microscopic nature of the adsorbate states, however, could not be clarified from the experimental information. Only in a close collaboration with theory, the structure of the molecular H_2 adsorption state on Pd(210) could be resolved[45,47].

The geometry of the (210) surface is indicated in Fig. 8. The (210) surface can be regarded as a stepped surface with a high density of steps[82]. Vicinal fcc(n10) surfaces have (100) terraces with steps running along the [001] direction. These steps are forming open (110)-like microfacets. The calculations showed that indeed this long-bridge position between two Pd step atoms (dark balls in Fig. 8) are the most favorable adsorption sites for atomic hydrogen with an binding energy of 0.52 eV, although usually hydrogen prefers highly-coordinated adsorption sites at metal surfaces[72]. This preferential adsorption on the low-coordinated step sites can be traced back to the upshift of the local d-band center at these first layer atoms (see Fig. 3). However, on the level of accuracy of the DFT calculations the long-bridge position is practically degenerate with the quasi-threefold position on the small terraces of the (210) surface. In spite of the fact that there is mutual repulsion between the adsorption hydrogen atoms on Pd(210), in fact another two hydrogen atoms can be adsorbed within the (210) surface unit cell at terrace sites[45,47].

In order to identify the nature of the experimentally found adsorbed H_2 species, the potential energy surfaces for the H_2 dissociation at clean and hydrogen-covered Pd(210) were evaluated. On clean Pd(210), H_2 dissociates spontaneously without any hindering adsorption barrier, like on the low-index palladium surfaces[79–81]. However, once the long-bridge sites at the steps are occupied by hydrogen atoms, a barrier for the dissociative adsorption builds up although hydrogen adsorption is still exothermic. This hydrogen precoverage leads to a metastable H_2 molecular chemisorption state above the Pd step atoms with a binding energy of 0.27 eV[45,47]. This molecular state is also illustrated in Fig. 8.

The preadsorbed atomic hydrogen does not significantly disturb the interaction of the H_2 molecules with the step Pd atoms but hinders the H_2 dissociation on Pd(210). This can be deduced from an analysis of the charge density. In Fig. 9, the total charge (a) and the charge density difference (b) are plotted in a plane formed by the surface normal and the [001] direction along the step atoms (compare with Fig. 8). First of all, it is obvious that an inspection of the total charge density (Fig. 9a) is not very instructive: the charge density is just concentrated around the atomic positions. In contrast, the plot of the charge density difference (6), i.e., the adsorption-induced change of the charge density (Fig. 9b), reveals that there is a strong charge rearrangement upon the H_2 adsorption on the hydrogen-covered Pd(210) surface. Regions of reduced electronic density (i.e., positively charged) compared to the isolated systems H_2 and H/Pd(210) are marked with a minus sign, regions of enhanced electron density with a plus sign. From the pattern of the charge redistribution around the Pd atom the hybridization of the H_2 molecular orbitals with the Pd d-states and its strong polarization can be infered. The polarization of the adsorbed H_2 molecule also leads to a large decrease of the work function which is confirmed by experiment[47].

The charge density difference plot also indicates that there is no direct hybridization between the adsorbed H_2 molecule and the pre-adsorbed hydrogen atoms at the step sites. This means that the H_2 molecular adsorption state is not stabilized due to any direct interaction between the molecule and the hydrogen atoms. The hydro-

gen atoms rather block the dissociation channel without influencing the interaction between the H_2 molecule and the Pd step atom so that the H_2 molecule can stay in the metastable molecular adsorption state.

In fact, the molecular adsorption state corresponds locally to the stable PdH_2 complex found in the gas-phase[77,83]. This unique feature of a nanostructured surfaces might be useful for catalyzing certain reactions in which, e.g., relatively weakly bound hydrogen molecules are required. DFT calculation also predict a molecular hydrogen state on hydrogen-covered Pd(100)[84], as will be discussed in section 7 of this review. At this surface, the hydrogen atoms are adsorbed in the four-fold hollow sites at about the same height as the neighboring Pd atoms so the the Pd atoms are still exposed enough to form a PdH_2. However, the H_2 binding energy is only 0.1 eV so that rather low temperatures are required to populate this state.

Palladium is known to be able to absorb large amounts of hydrogen which is important in the context of hydrogen storage and technology[85]. Therefore the subsurface absorption as the first step for the hydrogen dissolution into the bulk is also of particular interest. On Pd(210), the binding energy of hydrogen in the octahedral subsurface site is 0.21 eV, i.e. significantly lower than on the surface. This means that hydrogen prefers to stay on the surface. Only if the surface is fully covered with hydrogen, absorption into the bulk starts[47]. Furthermore, the hydrogen subsurface binding energies at the open Pd(210) surface and at the low-index Pd(111), Pd(111) and Pd(110) are basically the same. The open structure of the steps does apparently not play a significant role in the subsurface absorption. Because of the small size of the hydrogen atom, the substrate relaxations induced by the hydrogen subsurface absorption are only relatively small and limited to the first layer[45].

In addition, the CO adsorption on Pd(210) was addressed by DFT calculations[86]. Interestingly, CO does not preferentially bind to the step sites, but rather to the bridge sites at the small terraces with binding energies of 1.86-1.88 eV. These results can be understood considering the fact that CO is known to prefer bridge sites on Pd(100)[87,88] and near-bridge sites on Pd(110)[89–91]. At the steps, the CO molecule cannot find such a favorable adsorption geometry. As far as the CO adsorption site is concerned, the DFT calculations are in agreement with electron stimulated desorption ion angular distribution (ESDIAD) measurements[92] at low coverages up to $\theta = 1$ which suggest CO adsorbs in a bridge-bonded position, inclined away from the surface normal. Thermal desorption results yield an initial adsorption energy of 1.52 eV[93] or 1.45 eV per CO molecule[94]. Thus the calculated CO binding energies on Pd(210) seem to be overestimated. This is a well-known phenomenon, GGA calculations using the PW91 exchange-correlation functional tend to overestimate the CO adsorption on a wide range of metal surfaces[95].

The adsorption on (n10) surfaces was also the subject of a number of experimental and theoretical studies for the O/Ag system. Using molecular beam techniques and high-resolution electron energy loss spectroscopy (HREELS), Rocca and coworkers found that the steps of the Ag(210) and Ag(410) surface represent the active sites for the dissociative adsorption of O_2[96–98].

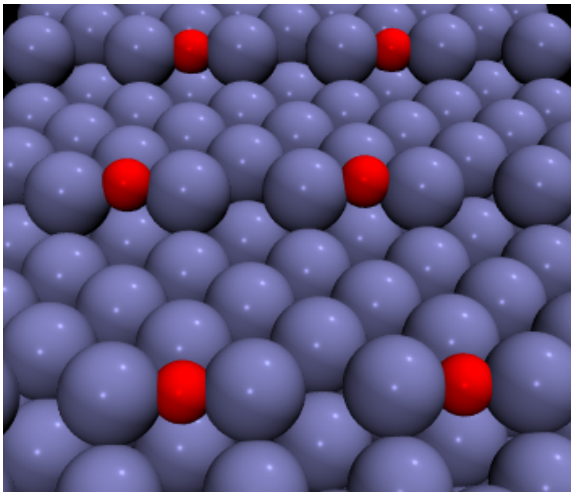

FIG. 10: Optimized geometries of oxygen atoms adsorbed in a (2×1) structure at the step sites of a Ag(410) surface[99].

Motivated by these experimental findings, the configuration of the most stable atomic oxygen adsorption sites on Ag(210) and Ag(410) was addressed in a DFT study[99]. The structure of oxygen atoms adsorbed in a (2×1) structure at the step sites of a Ag(410) surface, corresponding to a coverage of $\theta_O = 1/2$, is illustrated in Fig. 10. The results with respect to the binding energies of the oxygen atoms at step (S) and terrace (T) sites are summarized in table I. The given coverage θ_O is related to the number of oxygen atoms per (n10) surface unit cell. At the Ag(210) surface, the adsorption at the step sites is preferred compared to the terrace sites, as for H/Pd(210)[45], while on Ag(410) the adsorption energies are very similar at the step and the terrace sites. The subsurface incorporation of oxygen at the octahedral site of Ag(210) is

site	oxygen coverage θ_O	Binding energy E_b(eV) Ag(210)	Ag (410)
S	1/2	0.68	0.75
T	1/2	0.49	0.80
S	1	0.80	0.86
T	1	0.42	0.79
O_d	1/2	0.07	–
2S + O_d	3/2	0.54	0.55

TABLE I: Binding energy of oxygen atoms in eV/atom on Ag(210) and Ag(410) at step (S) and terrace (T) sites[99] and at the octahedral subsurface site O_d[100]. The coverage θ is related to the number of oxygen atoms per (n10) surface unit cell. For the last adsorption configuration, the adsorption energy corresponds to the average value.

energetically much less favorable than oxygen adsorption on the surface, again similar to H/Pd(210), but here it is mainly caused by the strong lattice distortion upon oxygen subsurface absorption[100].

However, the subsurface sites become stabilized when a sufficient amount of oxygen atoms is present on the surface[100], as the entries in table I for the configuration denoted by 2S + O_d demonstrate. This structure corresponds to steps fully decorated by oxygen atoms and one subsurface oxygen atom per (2×1) surface unit cell.

Another rather interesting result, however, is the increased stability of the oxygen atoms when they fully decorate the steps in a (1×1) geometry. This is in fact surprising because the negatively charged oxygen atoms experience a electrostatic repulsive interaction. For example, on Pt(211) where oxygen atoms also bind preferentially to the step sites, the (2×1) structure is more stable by 0.48 eV/adatom compared to the (1×1) structure[63] where every step site is occupied. Using density-functional perturbation theory, the vibrational spectrum of oxygen atoms on Ag(210) was evaluated[101]. The mixed on-surface/subsurface adsorption configuration exhibits a vibrational mode of 55 meV due to the coupled vibration of on-surface and subsurface oxygen atoms which is close to the one observed in the HREELS experiments[98].

An inspection of Fig. 10 reveals that the oxygen atoms are almost at the same height as the adjacent Ag atoms. this means that they are effectively screened from each other by the Ag step atoms. However, this fact alone can not explain the higher stability of the fully decorated steps. In fact, the authors of the computational study[99] do not have a water-proof explanation for this phenomenon. They believe that the mechanism causing this stability could be related to the arrangement of the O adatoms in O-Ag-O chains at the upper sides of the (110) steps. Such chains are for example also found in the added-row reconstruction of Ag(110)[102] and Cu(110)[103,104], upon oxygen adsorption.

As far as the oxygen position in the (2×1) and the (1×1) structures are concerned, for the high coverage the oxygen atoms are even closer to the surface than for the low coverage. Thus the Ag and O are almost aligned at the same height. Although there is some hybridization between the oxygen and the silver electronic states, there is a significant charge transfer only from the silver atoms at the steps to the oxygen atoms, leading to a electrostatically stable chain of atoms with alternating charges in the (1×1) structures. Interestingly enough, in the (2×1) structure the charge transfer from the terrace atom to the oxygen atom is very similar to the transfer from the step atoms. Hence, the electrostatic rearrangement is not restricted to the step atoms. Certainly, the stability of the oxygen-decorated Ag steps deserves further investigations.

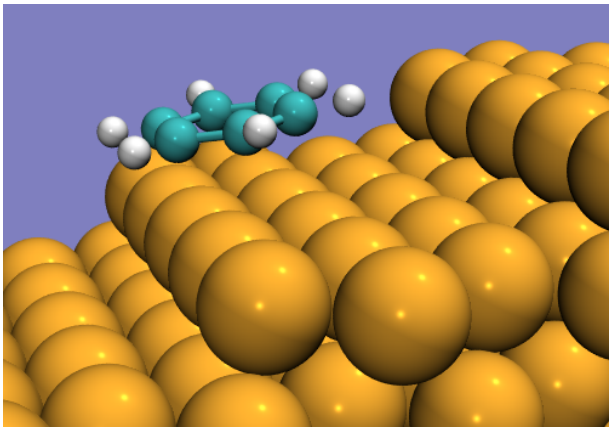

FIG. 11: Optimized structure of benzene, C_6H_6, adsorbed above a stepped Ni(221) surface according to DFT calculations[105]. The center of mass of the benzene molecule is shifted by about 1.0 Å from the step edge.

3.3. Adsorption of organic molecules on stepped surfaces

The molecules treated in the studies discussed above, such as CO or O_2, are relevant for many catalytic reactions, but still rather simple. However, organic molecules are also very often involved in reactions occuring in heterogeneous catalysis[107]. Hence the interaction of organic molecules with nanostructured surfaces is of considerable interest. As far as the description of the adsorption of organic molecules within DFT is concerned, one faces a certain dilemma: on the one hand, the quantum mechanical treatment of extended and complex substrates is only possible employing DFT; on the other hand, organic molecules are often bound via weak van der Waals or dispersion forces which are not well-described within DFT. Either one addresses only organic adsorbates that form strong chemical bonds with the substrate, or for weakly bound systems, the DFT energies have to be taken with caution. There are in fact ways to incorporate van der Waals forces in periodic DFT calculations, either by adding an explicit, empirical van der Waals contribution to the total energy[108], or by employing a hybrid quantum mechanical approach in which the dispersion effects for an extended system are derived from high-quality quantum chemistry calculations of a properly chosen cluster representing a finite section of the extended system[109–111]. However, the examples presented in this review have been addressed without such a correction.

Benzene (C_6H_6) corresponds to an aromatic π electron system. It binds to a nickel surface by forming bonds between the carbon and the metal atoms which are satisfactorily reproduced in DFT calculations. This was shown in a computational study that addressed the interaction of benzene with a stepped Ni(221) surface[105]. The most stable adsorption position of benzene is illustrated in Fig. 11. The center of mass of the carbon rings

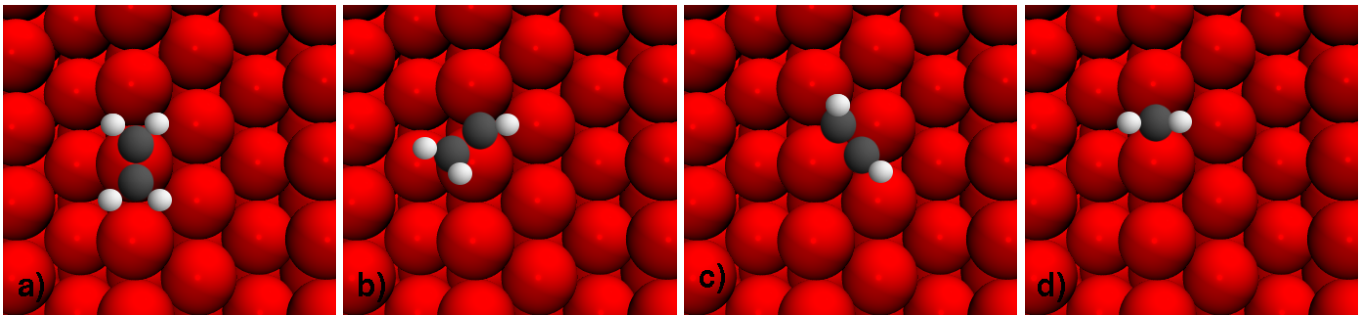

FIG. 12: Calculated adsorption geometries of (a) ethylene (C_2H_4), (b) vinyl (C_2H_3), (c) acetylene (C_2H_2), and (d) methylene (CH_2) on Ni(211) (after [106]).

is situated 1.0 Å away from the step edge. At this site, the binding energy of benzene, $E_b = 1.37$ eV, is enhanced by about 0.3 eV with respect to the value for the flat surface, $E_b = 1.05$ eV, and also with respect to the one for the center of mass of the benzene directly above the step edge.

The carbon-hydrogen bonds are bent slightly upwards, as Fig. 11 shows. This suggests that there is a repulsive interaction between the hydrogen atoms and the nickel substrate. This interpretation is supported by the fact that the binding energy of benzene to Ni(221) is further decreased by another 0.3 eV if the benzene molecule is shifted close to the step edge from below so that the hydrogen atoms directly interact with the Ni step atoms. The energetically most favorable adsorption position near the step allows the formation of strong bonds between the carbon ring and several nickel atoms. However, a shift of the molecule parallel to the surface hardly affects the binding energies. This seems to indicate that it is not the local bonding configuration at the step but rather the specific electronic properties of the step that cause its higher reactivity. And indeed, an analysis of the electronic structure shows that the polarization effects are more pronounced at the steps which leads to a larger charge transfer from the Ni atoms to the bonding region and thus to stronger bonds[105].

Employing the step-blocking technique, STM experiments showed that the decomposition of ethylene (C_2H_4) on Ni(111) is dominated by step edges[106,112]. In order to gain a detailed knowledge of the influence of the step edges on the ethylene-Ni interaction, DFT calculation of the ethylene decomposition reaction path on Ni(111) and Ni(211) were performed[106,112]. Whereas the steps of the (221) surface consist of triangular (111)-microfacets, the (211) surface has square (100)-microfacets at the steps. The adsorption geometries of the intermediates in the ethylen decomposition on Ni(211) are shown in Fig. 12. Ethylene adsorbs on a top site at the step with a binding energy of 0.76 eV that is 0.6 eV higher than on the terraces. All other intermediates also exhibit a stronger binding to the steps than to the (111) terraces.

The transition state energies for ethylene dissociation (C-C bond breaking) and dehydrogenation (C-H bond breaking) with respect to the free ethylene molecule in the gas phase are lower by more than 0.5 eV compared with the lowest barrier (dehydrogenation) on Ni(111) (see Fig. 13). However, with respect to the adsorbed ethylene molecule, the activation barriers for ethylene dehydrogenation to vinyl (C_2H_3) are similar on Ni(111) and Ni(211). Still, the dehydrogenation rate at the steps will be much larger since the ratio between the rates for dehydrogenation and desorption is much more favorable at the steps. This is similar to the case of O_2/Pt(211) discussed above.

Even more interestingly, the activation barrier for ethylene dissociation into two adsorbed methylene radicals (CH_2), which is much higher than the barrier for dehydrogenation on Ni(111), becomes comparable to the dehydrogenation barrier at the steps. This is caused by the fact that in the C-C bond breaking the final states, the methylene radicals, end up in two-fold sites at the reactive step (see Fig. 12d), whereas on the less reactive Ni(111) surface CH_2 prefers three-fold coordinated sites,

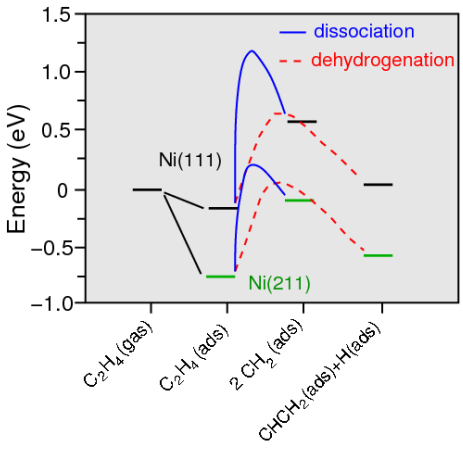

FIG. 13: Potential energy diagram of the initial steps of the C-C bond breaking (dissociation, blue line) and the C-H bond breaking (dehydrogenation, dashed red line) of ethylene on Ni(111) and Ni(211) (after [112]).

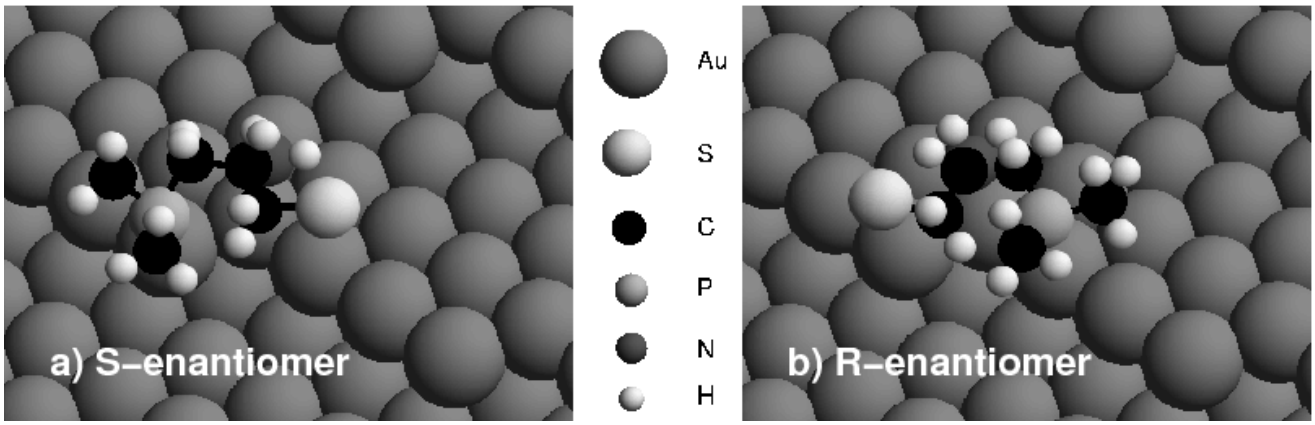

FIG. 14: Most stable adsorption configurations for the S-enantiomer (a) and the R-enantiomer (b) of APPT on Au(17 11 9)^S as determined in DFT-GGA calculations (after [113]).

and the CH_2 groups are stabilized at an earlier point on the dissociation path towards the two-fold bridge sites than towards the three-fold sites. This has the important consequence that at the Ni steps not only the transition state energies are lowered but that also the selectivity towards ethylene dissociation/dehydrogenation is strongly modified. Thus by creating specific defect sites, the selectivity of a certain reaction can be controlled.

An enhancement of ethylene binding energies at the steps of a metallic surface has also been found on stepped Ag surfaces in DFT calculations[114,115]. While ethylene hardly binds at the flat Ag(001) surfaces, the binding energy at the step sites of a Ag(410) is 0.25 eV. This stronger binding was attributed to the enhanced hybridization between the silver d and the ethylene π^* states at the steps. It should be noted, however, that probably the DFT binding energies are too low compared to the experiment due to the improper representation of dispersion forces in common DFT functionals.

The issue of chirality and so-called stereoselectivity of organic molecules on stepped surfaces had been addressed in a very ambitious DFT study[113]. High-index surfaces of fcc crystal with kink sites at the steps lack symmetry apart from translational symmetry if the step lengths or step faces on the two sides of the kink are not equal[116]. They are in fact chiral which means that two such surfaces which are created by reflection can not be superimposed on each other, and the kink sites are either left- or right-handed. The (643) surface exhibits this chirality, another example is the (17 11 9) surface which is illustrated in Fig. 14. In fact, in Fig. 14 the (17 11 9)^S = ($\bar{1}$7 11 9) surface is shown whereas the (17 11 9)^R = (17 11 9) is its enantiomorph that possesses the opposite chirality.

The chirality of organic molecules is actually rather important for molecular recognition and interaction. And the existence of chirality in kinked single crystal metal surfaces suggests that the adsorption and reaction probabilities of chiral molecules on these surfaces should be stereoselective, i.e. they should depend on the chirality of the molecules. Indeed, such a selectivity has been found, for example in the interaction of glucose with Pt(643)[117].

The first DFT study of the adsorption of a chiral molecule on a chiral surface was performed for the S and R enantiomers of 2-amino-3-(dimethylphosphino)-1-propanethiol (APPT, $HSCH_2CHNH_2CH_2P(CH_3)_2$) on Au(17 11 9)^S[113]. This particular molecule was chosen because in previous studies it was shown that their thiolate, phosphino, and amino groups are all able to bind to gold surfaces[118,119]. The two most stable adsorption sites of the S and R enantiomers of APPT on Au(17 11 9)^S are shown in Fig. 14. Their binding energies are 0.9 eV and 0.8 eV, respectively, i.e. there is an enantiospecifity in their binding. In the energetically most favorable configurations APPT binds indeed with its thiolate, phosphino, and amino groups to the gold atoms. By performing model calculations for the three groups separately it was shown that the binding of APPT to Au(17 11 9)^S can be understood in terms of these three local bonds plus the deformation energies of the molecule and the surface, respectively.

In the most favorable adsorption configurations, the molecular deformation is rather small. The enantiospecific binding rather results from the ability or inability to simultaneously optimize three local bonds between the molecule and the surface. While the S-enantiomer of APPT is able to find such an optimal adsorption configuration, the R-enantiomer is less favored because it is not capable of optimizing neither the thiolate-gold nor the amino-gold bonds. This fits into the picture that chiral recognition might be in general driven by the formation of three-point contacts[120] which represent the smallest number of contact points able to discriminate between two different enantiomers.

Interestingly enough, for two other related chiral molecules, the naturally occuring amino acid cysteine ($HSCH_2CHNH_2COOH$) and 2,3-diamino-1-propanethiol (DAPT, $HSCH_2CHNH_2CH_2NH_2$), no enantiospecific

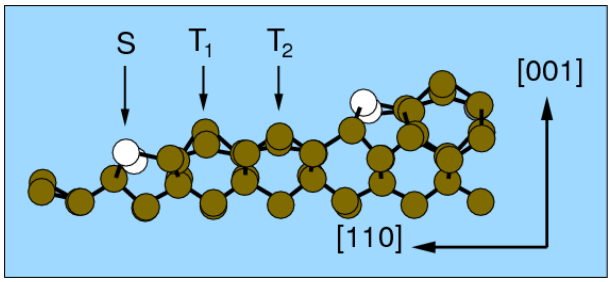

FIG. 15: Relaxed structure of the Si(117) surface with rebonded D_B steps according to DFT calculations[127]. The rebonded Si atoms are shown in white. The step and terrace atoms are denoted by S and T, respectively.

binding was found. For cysteine the lack of stereoselectivity in the adsorption on Au(17 11 9)^S is obviously related to the fact that it only binds on Au(17 11 9)^S through two groups, its thiolate and amino groups. DAPT, however, has three groups that form bonds with the surface, but two of them, the amino groups, are equal. Thus it is apparently important for the chiral behavior that all three molecule-surface bonds are different. This suggests that the character of the functional group mediating the binding is crucial for enantiospecific behavior.

3.4. Adsorption on stepped semiconductor surfaces

So far, we have exclusively considered the adsorption of atoms and molecules on stepped *metal* surfaces. However, semiconductor surfaces are also of considerable technological importance in the context of information technology, in particular Si surfaces. Especially the H_2/Si system has attracted a lot of attention[121] since hydrogen adsorption leads to a passivation of the surface. Furthermore, hydrogen desorption is the rate determining step in the growth of silicon wafers from the chemical vapor deposition (CVD) of silane.

On the flat Si(100) surface, the dissociative adsorption of H_2 is hindered by a barrier of the order of 0.4 eV according to DFT slab calculations[122,123], although the exact value of this barrier is still debated[124–126]. However, it was found experimentally that the hydrogen sticking coefficient at steps of vicinal Si(100) surfaces is up to six orders of magnitude larger than on the flat terraces[127].

As far as stepped semiconductor surfaces are concerned, it is important to realize that the termination of semiconductor surfaces is usually much more complicated than those of metal surface. This is caused by the covalent nature of the binding in semiconductors which strongly favors directional bonding and leads to extended reconstruction patterns[15]. At the conditions of the experiment, vicinal Si(100) surfaces have steps with a double-atomic height, the so-called rebonded D_B steps, which have additional Si atoms attached to the steps[128]. There are two electronic surface bands formed from the dangling bonds located at the rebonded Si atoms which are split by approximately 1 eV due to a Jahn-Teller mechanism[129,130] similar to the splitting observed for the Si dimer at the flat Si(100)-(2×1) surface.

The vicinal substrate was modeled by a Si(117) surface[127,131] whose structure is shown in Fig. 15 with the rebonded Si atoms shown in white. The calculations found that the step sites bind hydrogen atoms more strongly than the terrace sites by about 0.1 eV, similar to a Si surface with so-called rebonded single atomic height S_A and S_B steps[131]. However, the influence of the steps on the H_2 dissociation barrier is much more dramatic on the D_B steps. While the barrier heights are 0.40 eV and 0.54 eV at the terrace sites T_1 and T_2, respectively, H_2 molecules approaching the steps dissociate spontaneously, i.e., without any barrier, towards the Si rebonded atoms[127]. The high reactivity of the steps with respect to H_2 dissociation is caused by the fact that the splitting of the electronic bands is reduced to 0.4 eV when the H_2 molecule is approaching so that the surface states can interact efficiently with the molecular orbitals of the H_2 molecules. Hence the dissociation process involves some relaxation of the Si atoms with the asymmetry of two adjacent rebonded Si atoms being lifted. At the flat Si(001) surface, the π interaction between the dangling bonds prevents the two surface bands from coming closer to each other which makes the terrace sites less capable of breaking the H-H bond.

Scanning tunneling microscope (STM) experiments demonstrated that predosing the Si(100) surface by *atomic* hydrogen creates active sites at which the H_2 adsorption is considerably facilitated[132,133]. Interestingly enough, the mechanism for this enhanced reactivity of the hydrogen-precovered surface with respect to additional hydrogen dissociation is the same as at the steps since since the electronic structure of the dangling bonds is perturbed in a similar way by both steps and adsorbates[134]. These findings have also finally resolved the so-called barrier puzzle for the H_2/Si system[123,126]: While the sticking coefficient of molecular hydrogen on Si surfaces is very small[135,136] indicating a high barrier to adsorption, the low mean kinetic energy of desorbed molecules[137] suggests a small adsorption barrier. This puzzle arises from the fact that for the system H_2/Si the hydrogen coverage has a crucial influence on the H_2 dissociation barrier heights. Hence adsorption experiments that are usually performed in the low-coverage regime and desorption experiments which are carried out in the high-coverage regime probe different barriers.

4. ADSORPTION ON SUPPORTED CLUSTERS

4.1. Reactivity of supported clusters

Clusters are particles with sizes typically between a few and several thousands of atoms. They are characterized by the reduced dimension of the particle, a large surface

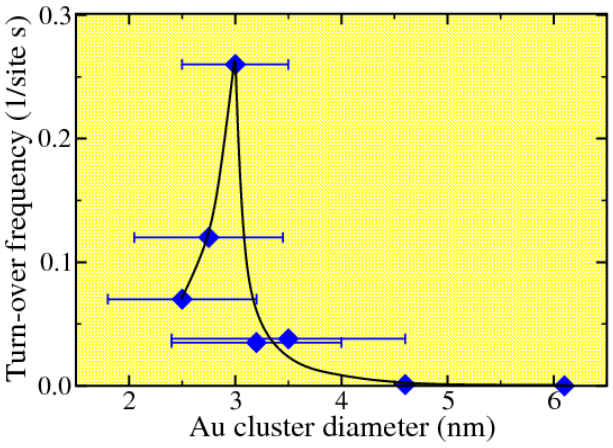

FIG. 16: Measured CO oxidation turnover frequencies at 300 K as a function of the average size of Au clusters supported on a high surface TiO_2 support. The solid line is meant as a guide to the eye (after [141]).

to volume ratio and a large number of low-coordinated atoms at edge sites. The properties of clusters lie usually between those of single atoms or molecules and those of bulk material. However, often small particles or clusters in the nanometer range show surprisingly strongly modified electronical, magnetic, optical and chemical properties which can be characterized by saying that small is different and that "every atom counts"[138]. Yet, it is often not clear whether the specific properties are caused by the reduced dimension of the particles ("quantum size effects") or by the large surface area of the nanocluster exhibiting many low-coordinated atoms or defect sites.

For technological applications, free clusters that are typically studied in molecular beam experiments are in general not very useful; they rather have to be fixed in space, either in a bulk matrix, as for example the so-called nanodots or quantum dots in semiconductor technology, or on a surface. These embedded or supported clusters can interact considerably with their environment so that the influence of the support can not be neglected for a proper theoretical description of the properties of the clusters. In fact, for metal clusters on surfaces the so-called strong metal support interaction (SMSI) has been discussed intensively[139,140] which significantly influences the catalytic properties of group VIII metals such as Fe, Ni, Rh, Pt, Pd, and Ir supported on metal oxides.

In recent years, supported gold clusters have become the prototype system for the study and understanding of the modified chemical properties of nanoscale structures. While gold as a bulk material is chemically inert, mainly due to its energetically low-lying, completely filled *d* band[35], small Au clusters show a surprisingly high catalytic activity, especially for the low-temperature oxidation of CO[141,142], but also for NO oxidation, the partial oxidation of propene, and the partial hydrogenation of acetylene. The size dependence of the CO oxidation turn over frequency, i.e., the reaction rate per surface Au site per second, is strongly peaked at about 3 nm which corresponds to $\sim$ 300 atoms per cluster (see Fig. 16). It should be noted that these clusters are rather flat with a height of only about two to three atomic layers. Additional scanning tunneling microscopy/spectroscopy experiments showed that the catalytic activity is related to size effects with respect to the thickness of the gold islands: two-layer thick islands are most effective for the CO oxidation[141]. At this cluster size also a band gap opens up with decreasing cluster size, i.e., a metal-to-nonmetal transition occurs.

Still the reasons for the large difference in the properties between bulk material and supported clusters are far from being fully understood. Several factors have been discussed so far that could be responsible for the difference: particle roughness, size dependence of the band gap, finite size effects or charge transfer phenomena.

Of course, these open questions have raised the interest of theoreticians in the properties of supported gold clusters[143]. Although the clusters treated in theoretical and computational studies are often much smaller than the ones studied in experiments, still some important qualitative aspects about cluster-adsorbate interaction can be learned from the theoretical studies as will be shown in the following.

4.2. Gold nanostructures

In fundamental studies, the interaction of oxygen atoms and molecules with free gold clusters and with flat and stepped Au surfaces was addressed[144–148]. Some of the results are summarized in Fig. 17 where O and O_2 adsorption energies on Au clusters and surfaces are plotted as a function of the coordination number of the Au atoms. The strong dependence of the adsorption energies on the coordination number is obvious. The results show the expected general trend that the binding is the stronger, the lower the coordination of the Au atoms is. Analogous trends have been also found in DFT calculations for CO adsorption on stepped Au surfaces and an Au adatom on Au(111)[149].

However, not all results can be explained with the coordination number alone. The O_2 binding to Au(111) is stronger than to Au(211) although the coordination number of the Au atoms in the (111) surface is higher. Similarly, Liu *et al.*[151] have found that O atoms bind stronger to a Au(211) surface (coordination number 7) than to a kinked Au(211) surface (coordination number 6). For an oxygen atom on a Au adatom on Au(111) (Au/Au(111), coordination number 3), they even found that the *atom* is not stable with respect to the associative desorption of O_2 into the gas phase which is surprising since O_2 *molecule* are bound to Au/Au(111)[144]. Apparently, the coordination number is an important parameter in order to understand the interaction of atoms and molecules with specific sites, but there are other parameters such as the nature of the orbitals involved in the bonding[144]

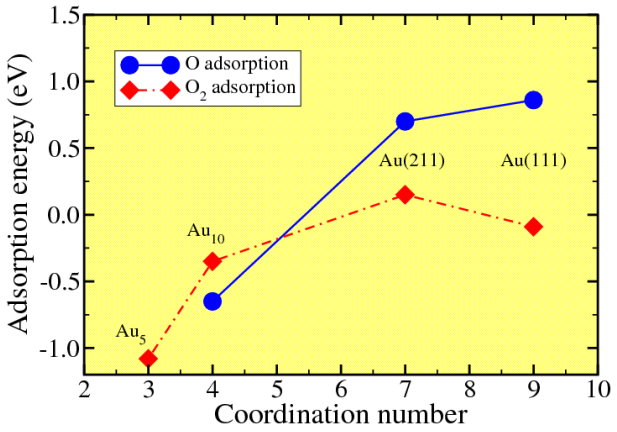

FIG. 17: Adsorption energies of O and O_2 on a Au_{10} cluster, on Au(211) and Au(111) plotted as a function of the coordination number of the Au atoms (after [147]). In addition, the results for the O_2/Au_5 and O_2/Au(111) by Mills *et al.*[144] are included. All the results have been obtained by DFT calculations using the PW91 functional[150].

that are crucial for a complete understanding.

4.3. Bonding of nanoparticles to oxide substrates

In order to make closer contact with the experiments of Au clusters supported by oxide substrates, the adhesion and shape of Au atoms and clusters on oxide surfaces has been addressed by several authors from a theoretical point of view[152–157]. The calculations showed that the interaction of single gold atoms[152] and of a monolayer of gold with a perfect rutile $TiO_2(110)$ surface[154] is rather small. Thus it was concluded that the adhesion of gold to TiO_2 requires the presence of oxygen defects or possibly steps and adatoms. In a combined STM and DFT study, the adhesion of gold nanoparticles to $TiO_2(110)$ in three different oxidation states was addressed[157]. The considered substrates were either (i) reduced (having bridging oxygen vacancies), (ii) hydrated (having bridging hydroxyl groups), or (iii) oxidized (having oxygen adatoms).

Gold cluster Au_n	TiO_2 surface		
n	r-$TiO_2(110)$	h-$TiO_2(110)$	o-$TiO_2(110)$
1	1.14	0.54	2.38
2	0.71	0.05	1.94
3	1.41	1.26	3.09
4	0.57	0.64	4.04
5	0.31	1.04	3.57
7	0.52	0.87	3.83

TABLE II: Total binding energies in eV of the most stable Au_n clusters on the reduced (r-$TiO_2(110)$), the hydrated (h-$TiO_2(110)$) and the oxidized (o-$TiO_2(110)$) form of the $TiO_2(110)$ surface.

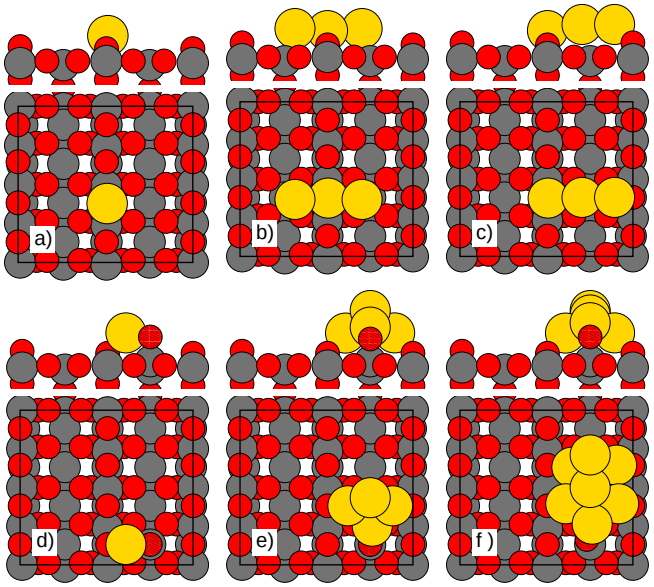

FIG. 18: Side and top views of the optimized structures found in DFT calculations for Au_n clusters with one Au atom above an O_{br} vacancy of the reduced $TiO_2(110)$ surface (a-c) and Au_n clusters attached to an oxygen adatom of the oxidized $TiO_2(110)$ surface (d-e) (after [157]). Grey circles: Ti, red circles: O, gold circles: Au. The oxygen adatom is additionally hatched. a) Au_1, b) symmetric Au_3 cluster, c) asymmetric Au_3 cluster, d) Au_1, d) Au_4, f) Au_7.

The binding energies of the most stable $Au_n, n = 1-7$ clusters on these three different surfaces are listed in Table II. The configurations of some of the most stable supported Au_n clusters are illustrated in Fig. 18. It is obvious that the Au_n nanoparticles are most strongly bound on the oxidized surface, o-$TiO_2(110)$, where they attach to the oxygen adatom (Fig. 18d-e). Furthermore, whereas the binding energies of the Au_n clusters on the reduced surface, r-$TiO_2(110)$, decrease with increasing cluster size, they are rather constant on o-$TiO_2(110)$.

In order to gain insight into the binding mechanism of the supported Au_n clusters, the electronic structure of the most stable clusters was analyzed. On the oxidized surface, electron charge is transfered from the Au clusters to the surface O atoms so that the cluster becomes cationic and the bonding between the Au_n clusters and o-$TiO_2(110)$ is partially ionic. In contrast, on the electron-rich reduced o-$TiO_2(110)$ and hydrated h-$TiO_2(110)$ surfaces the interaction is mediated through covalent bonds which do not lead to such a strong Au_n-support bonding.

The situation is apparently somewhat different for Au_n particles with $n = 1-3$ on the TiO_2 anatase (101) surface, as DFT calculations showed[153]. While the binding energies E_b of the Au_n particles on the stoichiometric surface are typically between 0.3 eV and 0.8 eV (with the exception of Au_3 adsorbed in a bent geometry having a binding energy of $E_b = 1.9$ eV), the binding ener-

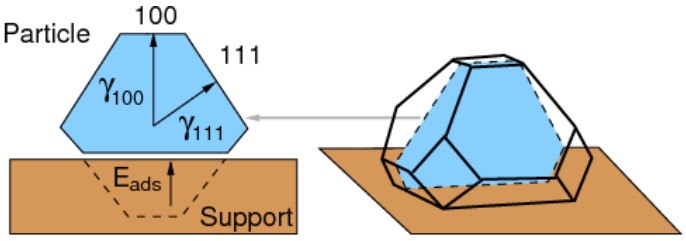

FIG. 19: Schematic illustration of a truncated Wulff polyhedron on a support. The left panel corresponds to a two-dimensional cut through the three-dimensional polyhedron in the right panel (after [155]).

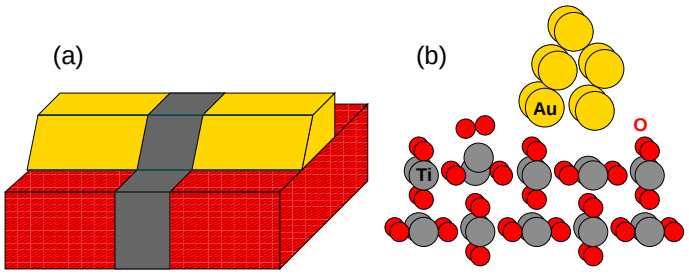

FIG. 20: Illustration of the one-dimensional rod model for the adsorption of O_2 an Au/TiO_2 nanoparticles used in GGA-DFT calculations. a) Schematic representation of the rod geometry. The dark-shaded area corresponds to the unit cell. b) Relaxed structure of O_2 binding at the Ti trough close to a supported one-dimensional Au rod with a sharp Au edge (after [156,158]).

gies of these clusters on the reduced anatase surface with an oxygen vacancy are between 1.8 eV and 3.6 eV[153]. The strong binding is accompanied by a relatively large charge transfer to the gold atoms. Interestingly enough, CO interacts much more strongly with clusters adsorbed on the stoichiometric surface than with clusters adsorbed on vacancies. This has been associated with the negative charge of the gold atoms which implies an unfavorable interaction with the dipole moment of the CO molecule[153]. However, it might also well be that the electrons involved in the strong bonding of the Au_n particles to the reduced surface are not available for the additional bonding of an adsorbate thus causing a weaker interaction.

Whereas the cluster considered in these DFT calculations are still rather small, the supported Au clusters studied in the CO oxidation experiments[141,142] are much larger. The size and the shape of macroscopic supported particles in thermal equilibrium can be derived from the Wulff construction[15] which is illustrated in Fig. 19: the particle is truncated in all directions at distances proportional to the interface or surface free energy of the crystal plane in that direction. This construction does not account for the formation energies for edge and corner atoms and is therefore only valid in the limit of large macroscopic crystals where the total formation energy of the edges is negligible compared to the total surface energies of the facets.

In order to take defect and edge effects into account, Lopez *et al.* also included defect and edge energies estimated from calculations of slabs containing one to four gold layers[154]. Thus they found that Au particles with a diameter of 3-4 nm, such as the ones studied in the experiments[141,142], are three to four layers thick. This means that the Au particles are in fact rather flat, in good agreement with the experiment.

4.4. Interaction of molecules with oxide-supported clusters

As just mentioned, the supported Au clusters used in the experiments in order to study the CO oxidation[141,142] are significantly larger than those accessible to first-principles electronic structure calculations where the number of clusters atoms is typically below 10. In order to still be able to investigate the binding of O_2 and CO to these clusters, Molina *et al.*[156] decided to model the interface between the nanoclusters and the substrate by replacing the nanoparticle with one-dimensional rods. One side of the rod was modeled according to the local bonding situation of the Au atoms at the edge of a nanoparticle while the other side of the rod only served the correct boundary conditions towards the interior of the supported clusters. This approach is illustrated schematically in Fig. 20a.

The adsorption studies are performed for $p(N\times2), N = 2, 3$ surface unit cells using four trilayer TiO_2 slabs. Such a large number of trilayers is indeed necessary because of the strong relaxation effects upon adsorption. Figure 20b shows a side-view of the relaxed atomic structure of the Au rod on TiO_2 with a sharp Au particle termination together with the optimal O_2 adsorption position (only the two uppermost trilayers are shown). Another rod with a more rounded termination has also been considered in the study (see Fig. 21).

DFT calculations show that on clean, stoichiometric $TiO_2(110)$, O_2 does not bind[159]. However, the adsorption of O_2 on top of a Ti trough atoms is strongly stabilized by the presence of a Au cluster with its edge above the adjacent bridging O atoms of the $TiO_2(110)$ surface (see Fig. 20), resulting in a binding energy of 0.45 eV. The O_2 adsorption is accompanied by a strong relaxation of the TiO_2 substrate with the Ti trough atom below the oxygen molecule pulled up by 0.8 Å. An analysis of the charge density distribution reveals a considerable charge transfer from the supported Au particle to the O_2 molecule mediated by the surface through electronic polarization. The bond length of the adsorbed O_2 molecule is enlarged to 1.41 Å, a value similar to the one for the peroxo O_2^{-2} species, which indicates that there is a significant charge transfer to the O_2 molecule.

Since TiO_2 is a reducible oxide, a TiO_2 substrate with a bridging oxygen vacancy in the $p(3\times2)$ surface unit cell was also considered in the calculations. On the clean

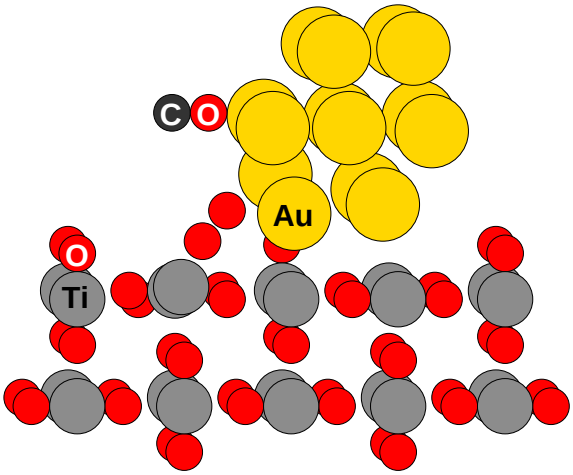

FIG. 21: Minimum energy structure of a leaning O_2 molecule and a CO molecule bound to a Au rod on TiO_2 with rounded shape and the oxygen vacancy situated below the nanoparticle edge (after [156]).

reduced TiO_2 surface, a O_2 molecule on the adjacent Ti trough atom becomes strongly bound by more than 1 eV. There is a significant charge transfer from the O vacancy to the O_2 molecule leading again to a peroxo O_2^{-2} species. The O_2 binding energy is even further increased to 1.65 eV if the edge of the Au rod is located above the O vacancy. This suggests that the Au rod provides additional charge for the binding of the O_2 molecule. The Au rod does in fact only weakly interact with the O vacancy so that the adsorption configuration is very similar to the one for the stoichiometric TiO_2 surface. This is different if a single Au atom is located at the vacancy site. Then the O_2 binding energy is reduced to 0.64 eV because of the competition between the O_2 molecule and the low-coordinated, reactive Au atom for the electrons of the vacancy[156].

As far as the CO oxidation is concerned, these O_2 species are all too strongly bound in order to serve as an initial state for an oxidation reaction. On the other hand, the Au rod with the sharp edge binds CO too weakly which is caused by the unfavorable orientation of the CO molecule with respect to the edge because of the presence of the substrate. Hence the sharp edge does apparently not promote CO oxidation. In contrast, the edge geometry shown in Fig. 21 provides a favorable structure. At the rounded edge, the CO molecule can bind strongly enough (~ 0.5 eV) to the low-coordinated Au atoms of the second layer. At the same time, a weakly bound O_2 species (binding energy $E_b = 0.1\,\mathrm{eV}$) exists in a leaning configuration. This O_2 molecule can approach the CO molecule and react with the CO to CO_2 in a Langmuir-Hinshelwood mechanism rather easily: the CO_2 formation is only hindered by a barrier of 0.15 eV, and the remaining O atom is left on top of a Ti trough atom.

However, it is fair to say that the exact mechanism for the low-temperature CO oxidation on titania-supported Au clusters has not been entirely clarified yet. For example, the oxidation state of the TiO_2 substrate that is favorable for the Au cluster adhesion and the CO oxidation is still debated[157], as discussed in the previous section. There are also further experimental results which demonstrate that gold monolayers and bilayers can completely wet, i.e. cover the titania support[160]. It was also found that the gold bilayer structure is significantly more active with respect to CO oxidation than the monolayer structure. This also means that the O_2 molecule involved in the CO_2 formation cannot bind to the TiO_2 substrate. In spite of the detailed investigations already performed for the Au/TiO_2 system, certainly further experimental and theoretical studies are needed to fully understand the exceptional activity of Au nanostructures supported on oxide substrates.

MgO represents another oxide substrate that has been used as a support for Au nanoparticles. In a collaboration between experiment and electronic structure theory, the CO oxidation catalyzed by size-selected Au_n clusters with $n \leq 20$ supported on defect-poor and defect rich MgO(100) films was investigated[10]. According to the experiments, gold clusters deposited on defect-rich MgO-films have a dramatically increased activity compared to clusters deposited on defect-poor films at temperature between 200 and 350 K. There is a significant size-dependence of the catalytic activity of the nanoparticles with the Au_8 cluster the smallest catalytically active particle.

LDA-DFT calculations using a finite presentation of the oxide substrate were performed in order to explore the microscopic mechanisms underlying the observed catalytic behavior[10]. Between 27 and 107 substrate atoms were embedded into a lattice of about $2000 \pm 2\,\mathrm{e}$ point charges at the positions of the MgO lattice. The defect-rich substrate was modeled as a MgO(100) surface with an oxygen vacancy, a so-called color center or F-center (from German "Farbzentrum") because of its optical properties. The equilibrium shape of a Au_8 cluster adsorbed on the defect-free MgO surface and on the F-center was determined and reaction paths of the CO oxidation catalyzed by the Au_8 cluster were explored. Figure 22 shows a side view of the Au_8 cluster adsorbed on the F-center. The structure corresponds to a deformed close-packed stacking. A sizable charge transfer of $0.5\,\mathrm{e}$ from the MgO(100) surface to the gold octamer has been found which is believed to contribute to the high catalytic activity of the Au_8 cluster.

In addition, a snapshot along the CO oxidation path according to an abstraction or so-called *Eley–Rideal mechanism* is shown in Fig. 22. A CO molecule approaches an adsorbed O_2 molecule and reacts spontaneously to form a weakly bound ($\sim 0.2\,\mathrm{eV}$) CO_2 molecule that can directly desorb plus an adsorbed oxygen atom. Another reaction pathway of the Langmuir-Hinshelwood type was also found with a similarly small barrier where the two reactants are initially coadsorbed on the top-facet of the Au_8 cluster. DFT calculations showed that

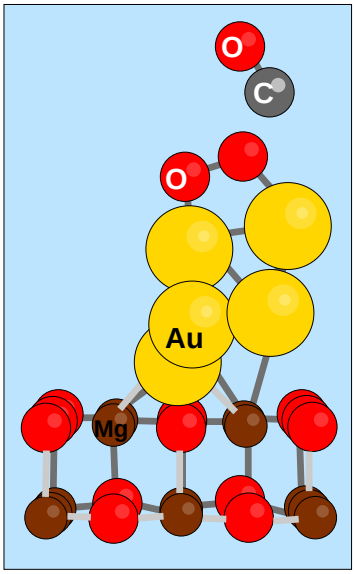

FIG. 22: CO oxidation on an Au_8 cluster adsorbed on a MgO(100) surface containing an oxygen-vacancy F-center. Due to the perspective, not all Au atoms are visible. A snapshot of a CO molecule approaching an adsorbed oxygen molecule is shown (after [10]).

the charge transfer from the F-center to the Au nanoclusters strongly correlates with a red-shift of the stretch frequency of CO coadsorbed with molecular oxygen[161], i.e., with a softening of the C-O bond. This means that the charge transfer activates the adsorbed CO molecule and thus promotes the CO oxidation.

Such reaction channels could explain low-temperature CO oxidation down to 90 K. As far as the higher-temperature oxidation is concerned, further channels have been identified at the periphery of the gold cluster. Their barriers are much smaller at the Au_8 cluster adsorbed above the F-center than on the perfect surface giving an explanation for the enhanced activity of the clusters on the defect-rich substrate. A similar effect has been found in a combined experimental and theoretical study addressing the reactivity of nano-assembled Pd catalysts on MgO thin films[162] where, however, the Pd catalysts were just modeled by single atoms in the calculations.

Another important aspect for the reactivity of small supported clusters is their dynamic structural fluxionality[163]. They are able to adapt their structure in order to provide energetically favorable adsorption sites. For the Au_8 cluster supported on the stoichiometric MgO(100) surface, it was indeed found that constraining the cluster to its original geometry prevents the adsorption and activation of O_2[163].

The CO oxidation at MgO supported gold aggregates was also addressed in a DFT study by Molina and Hammer[155,158] who particularly focused on the role of the oxide support for the CO oxidation. As a first step, the shape of adsorbed gold particles was determined using the Wulff construction which is illustrated for a two-dimensional cut in the left panel of Fig. 19. According to the calculated surface energies of Au low-index faces and the Au-MgO adhesion energies, the Au clusters assume a partial wetting shape as shown in the right panel of Fig. 19, in agreement with the experiment[164].

However, as already mentioned above, the Wulff construction does not account for the formation energies for edge and corner atoms and is therefore only valid in the limit of macroscopic crystals where the edge and corner energies do not play any role. For smaller clusters, the assumption of negligible total edge and corner energies is no longer justified. And indeed, Molina and Hammer found that the energetically most stable structure of a Au_{34} cluster on MgO does not look like the one shown in Fig. 19. The supported Au_{34} cluster rather shows a increasing degree of partial wetting, i.e., the cluster assumes a flat shape with a enlarged interface area between support and cluster.

Furthermore, the adsorption of CO, O_2 and the CO oxidation at the MgO supported gold aggregates were studied. Again, like in the study by Molina *et al.* of TiO_2 supported Au nanoparticles just discussed[156], the nanoparticles where replaced by an one-dimensional rod within a MgO(100)-(5×2) geometry. The calculations showed that the MgO support plays an active role in the bonding and activation of adsorbates bound to supported gold particles, however, this role is much less dramatic than for TiO_2[156] where the reduced substrate not only provides charge for the binding of the O_2 molecule but actually binds the O_2 molecule.

Experimentally, the oxide substrates are often prepared as thin films on metallic substrates so that probe techniques employing electrons can be used without charging effects[8]. However, the metal support of the oxide films can also have an influence on the adsorption properties of the oxide. DFT calculations predicted that for metal-supported MgO films that are thin enough (≤ 1 nm, of 4 to 5 MgO layers)) there is an enhanced adhesive bonding of Au_n clusters, $n = 8, 16, 20$, deposited on MgO films because of the electrostatic interaction between the underlying metal and the cluster-oxide interface[165]. According to the calculations, this interaction causes a wetting behavior of the Au, i.e., the formation of an Au film, in contrast to thick oxide film where Au forms clusters. The prediction of the crossover from three-dimensional cluster to two-dimensional film geometries of Au nanostructures on thin MgO(001) films with decreasing film thickness has in the meantime been confirmed in a STM study[166].

4.5. Metal-supported clusters

So far we have shown that the presence of low-coordinated sites at oxide-supported metal nanoparticle leads to a stronger interaction with adsorbates. However, there is another effect which can in fact counter-

balance the promoting effect of the low coordination of the nanoparticles, namely the interatomic relaxation of the small particles. This leads to reduced interatomic distances which, together with a strong cluster-support interaction, can cause a weaker binding of adsorbates[44].

In this section, we will consider metal nanoparticles that are supported by a noble metal such as Pd cluster on a gold substrate. These systems are of particular interest in the field of electrochemistry[167] because the substrate has to be conductive so that supported nanostructures can act as electrodes. The cluster can be deposited on the electrode using an electrochemical STM within the *jump-to-contact* technique[167–169]; thus highly ordered arrays of nanofabricated metal clusters containing of the order of only one hundred atoms can be generated. Some of these clusters exhibit in fact an unusual electrochemical stability, and it has been speculated that this stability might be caused by quantum size effects in the metal particles[167].

In order to understand the chemical and electronic properties of the Pd/Au particles, in a first step the binding energies of hydrogen and CO on pseudomorphic Pd/Au overlayers has been evaluated by DFT calculations[42,43]. These calculations demonstrated that both the expansion of the pseudomorphic overlayers by 5% as well as the relative weak interaction of the Pd overlayer with the gold substrate lead to a stronger interaction with the adsorbates compared to a bulk Pd substrate. Both effects, which can again be understood within the *d* band model, enhance the adsorption energies on Pd/Au(111) by a similar amount which is about 0.10-0.15 eV.

In a next step, the adsorption properties of small Pd_n cluster (n = 3,7,10) on Au(111) were evaluated using DFT[170]. In Fig. 23a, the nearest-neighbor Pd-Pd distances in these supported nanoparticles are analyzed. Note that the calculated nearest-neighbor distances in bulk Pd and bulk Au are 2.80 Å and 2.95 Å, respectively. In contrast, the Pd atoms of the Au-supported cluster have nearest-neighbor distances of 2.76–2.78 Å which is even below the Pd bulk value although adjacent three-fold hollow sites are 2.95 Å away from each other on Au(111). At the second layer of the Pd_{10} cluster, the Pd-Pd distances are even further reduced to 2.65 Å. These reduced distances are a consequence of the low coordination of the cluster atoms which makes the single Pd-Pd bonds stronger than in a bulk situation where every Pd atom is twelve-fold coordinated. For the free relaxed planar Pd_3 and Pd_7 cluster, the nearest neighbor distances are further reduced to 2.50 Å and 2.64 Å, respectively[170].

The DFT calculations show that these reduced Pd-Pd distances lead to a larger overlap of the *d* orbitals, a broader local *d*-band and consequently a down-shift of the local *d*-band center because of charge conservation[170] (compare with Fig. 2). According to the *d*-band model, this should result in smaller binding energies of adsorbates. This is indeed true as the adsorption energies for CO located at different sites of the Pd_{10} clusters supported by Au(111) plotted in Fig. 23b demonstrate. All

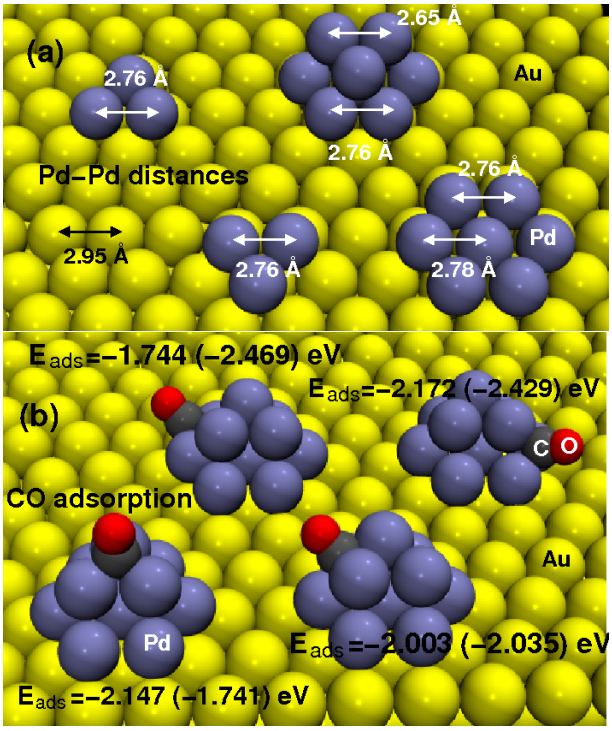

FIG. 23: Calculated nearest-neighbor Pd-Pd distances in Å of Pd_n cluster supported by Au(111) (a) and CO adsorption positions and energies on the Pd_{10}/Au(111) cluster (b). The energies in parentheses correspond to the adsorption energies on free Pd_{10} clusters in exactly the same configuration as the supported clusters (after [170]).

the CO binding energies are in fact lower than the corresponding value on a pseudomorphic Pd/Au(111) overlayer, $E_b = 2.3$ eV[42,43]. Obviously, in the Pd/Au system CO binds less strongly to low-coordinated clusters than to high-coordinated atoms in pseudomorphic overlayers. The same results have also been found for atomic hydrogen adsorption energies. This confirms that the Pd-Pd distances play an equally important role for the reactivity as the coordination of the Pd atoms on Au substrates.

The CO adsorption energies on free Pd_{10} clusters in exactly the same configuration as the supported clusters are also given in Fig. 23 by the numbers in parentheses. The corresponding binding energies are in fact larger than those on the supported clusters and also on flat[171] and stepped Pd surfaces[86]. This shows that in spite of their compression free clusters can still be much more reactive than surfaces because of their low coordination if they are not interacting with a support. Thus it is the interaction of the Pd clusters with the support that also contributes to the low binding energies on the metal-supported clusters.

Interestingly enough, at the top layer adsorption site of the Pd_{10} cluster, the CO binding energies on the free cluster are smaller than on the supported cluster. This surprising result is caused by the reactivity of the unsaturated hexagonal bottom layer of the free Pd_{10} cluster.

It binds the three topmost Pd atoms so strongly that the top layer becomes less reactive, as an analysis of the energetics and the electronic structure of the free cluster confirms[170].

As already mentioned, it has been speculated that the unusual electrochemical stability of nanofabricated supported metal clusters[168] could be caused by quantum confinement effects[172] that would lead to a discrete electronic spectrum in the clusters. However, the DFT calculations yield a continuous spectrum already for small supported Pd_3 clusters[170]. For larger clusters, any quantum confinement effects would even be smaller. Thus these calculations do not support the speculation of Ref. [172].

As an alternative explanation it has been proposed that the electrochemical nanofabrication of the clusters by the jump-to-contact technique leads to alloying of the clusters which causes their high electrochemical stability[173,174]. The deposition of the clusters has been simulated using classical molecular dynamics with the interatomic interaction described within the empirical embedded-atom-method (EAM)[175,176]. The stability of the deposited clusters was then analyzed by grand-canonical Monte Carlo simulations which took the electrochemical potential into account[177]. The simulations indicate that electrochemically stable clusters occur only in those cases where the two metals that are involved form stable alloys. In fact, DFT calculations also indicate that the Pd_{10} clusters on Au(111)[170] are stabilized by 0.1 eV if one of the Pd atoms at the base of the cluster is exchanged with an Au atom of the underlying substrate[178].

5. NANOSTRUCTURED SURFACE ALLOYS

5.1. Bimetallic surfaces

The metal-supported metal clusters just discussed are an example of a bimetallic system. Such systems are of strong interest in heterogeneous catalysis[179–181] and electrocatalysis[182] since they allow to modify their properties by altering its structure or its composition (or both)[44], preferentially in a rational manner. Many bimetallic systems that are immiscible in the bulk are still able to form alloys at the surface. These *surface alloys* can lead to a nanostructuring of the surface, exhibiting either only short-range[183] or also long-range order[184].

In order to discuss the activity of bimetallic catalysts, the concepts of the *ensemble* and the *ligand* effect are often used[179,185]. The term *ensemble effect* refers to the fact that for many reactions a certain number of active sites is required for a particular reaction to occur so that by blocking a large ensemble of active sites certain reactions can be suppressed. This can for example increase the selectivity towards reactions that only need a small ensemble of active sites. The catalytic activity of a bimetallic system is also modified by the electronic interactions between the components; this is called the *ligand effect*. In addition to this pure electronic effect, the modifications of the interatomic distances in a bimetallic system can also have a decisive influence on its electronic structure and thus on its catalytic activity. This *geometric effect* should also be considered together with the ensemble and ligand effects when the reactivity of bimetallic systems is discussed.

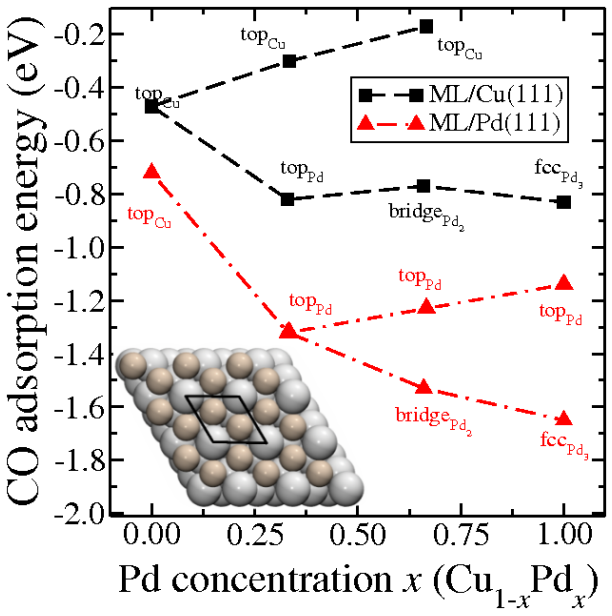

FIG. 24: CO adsorption energies on the top and the most favorable adsorption sites of CuPd monolayer surface alloys on Cu(111) and Pd(111) calculated as a function of the Pd concentration in the surface alloy[186]. The inset shows the structure of the ordered $PdCu_2$ surface alloy.

5.2. Ligand vs ensemble effects

The role of the ligand vs the ensemble effect in the interaction of CO with CuPd surface alloys on Cu(111), Pd(111) and Ru(0001) was studied by means of periodic DFT calculations[186]. The calculated CO adsorption energies at the top and the most favorable adsorption sites of CuPd monolayer surface alloys on Cu(111) and Pd(111) are shown in Fig. 24 as a function of the Pd concentration in the surface alloy. Note that Pd is usually catalytically more active than Cu since its *d*-band is not completely filled. The lower curves in Fig. 24 correspond to the adsorption energies at the most favorable adsorption sites which change from the Pd top site over the Pd bridge site to the three-fold coordinated Pd hollow site with increasing Pd concentration. The binding energies of CO to the PdCu surface alloy exhibits an ensemble effect: it becomes stronger with the availability of higher-coordinated Pd sites.

On the other, the binding energies at the ontop Cu and Pd sites decreases with increasing Pd concentration. This means that the *single* Cu and Pd atoms in this surface al-

loy interact less strongly with CO when the more reactive metal Pd is added. This surprising behavior is caused by a strain-mediated ligand effect. Pd has a lattice constant that is 8% larger than the one of Cu. Thus increasing the Pd concentration in the surface alloys whose interatomic distances are kept fixed by the underlying metal substrate induces a compressive strain in the surface alloy monolayer. This is the opposite scenario of the one depicted in Fig. 2: the compressive strain increases the band width which leads to a down-shift of the *d*-band and thus to a weaker interaction with adsorbates.

As a consequence, bimetallic surfaces do not necessarily show properties that that are intermediate between those of the pure components; instead, they can be beyond those of both components. For example, the binding energies of CO to the Cu top sites in CuPd surface alloys shown in Fig. 24 are lower than to the top sites of pure Cu and pure Pd surfaces. This behavior is especially pronounced if a more reactive metal with a smaller lattice constant is mixed with a less reactive metal with a larger lattice[44], as for example in PtRu[187–190], PdAu[42,43], PtAu[182,191], or RhAg[192] because then ligand and geometric effects both act in the same way.

6. NANOSTRUCTURING OF SURFACES BY ORGANIC MONOLAYERS

6.1. Organic template structures

So far we have only dealt with atomic and molecular adsorption *on* nanostructured surfaces. However, a nanostructuring of a flat surface can also be formed by ordered arrays of adsorbed molecules. In particular *organic* adsorbates can induce a nano-patterning in the form of ordered overlayers or molecular wires[193]. These nanostructures can then be used as templates for the deposition of functionalized molecules or for the assembly of higher ordered polymers in a host-guest approach. It has for example been suggested that the spontaneous self-assembly of DNA-base molecules on mineral template surfaces may play an essential role for the origin of life under prebiotic conditions[194,195]. Furthermore, these structure might also be technologically relevant in the context of sensing, catalysis, or molecular electronics.

Organic molecules adsorbed on inorganic substrates forming self-assemblied monolayers (SAMs) exhibit a rich variety of possible structures. However, the underlying principles responsible for the structure formation are still not fully understood. The structure of organic layers on surface are typically analyzed using the STM. Unfortunately, these STM images do often not have a true atomic resolution. Furthermore, STM images are not directly related to the geometric atomic structure but rather to the electronic structure of the surface, and the relationship between atomic and electronic structure of molecules and surfaces is not always trivial. One prominent example is the graphite(0001) surface where only every second carbon atom of the surface layer is imaged due to a purely electronic effect[196].

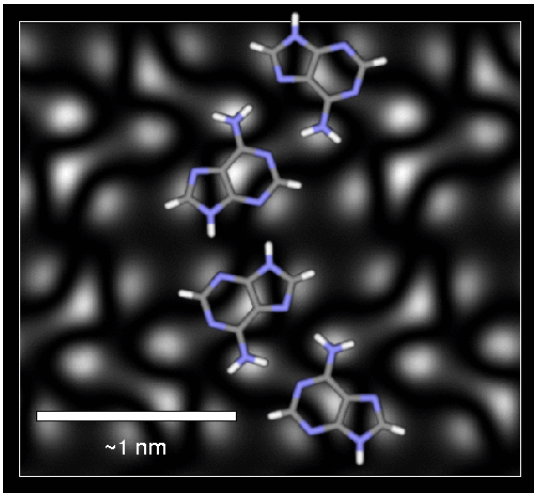

FIG. 25: Simulated STM image of adenine molecules according to the Tersoff-Hamann picture, i.e. the LDOS of the HOMO band is plotted. In addition, the underlying structure of the adsorbed adenine molecules is indicated (courtesy of T. Markert).

Within the Tersoff-Hamann picture[197], the tunneling current is simply proportional to the local density of states *of the surface* close to the Fermi energy at the position of the tip which is a standard information that can be taken from DFT calculations. Hence DFT calculations can contribute to the interpretation of STM images. There are more sophisticated DFT-based approaches to simulate STM images that also take into account the orbitals of the surface and the STM tip[198], but usually the simple Tersoff-Hamann picture is surprisingly successful and accurate.

Figure 25 shows a simulated STM image of the purine base adenine (6-aminopurine, $C_5H_5N_5$) together with the underlying geometric structure. The periodicity of the arrangement has been adjusted to results of low-energy electron diffraction (LEED) experiments[199]. The STM simulation just corresponds to the local density of states of the electronic band related to the highest occupied molecular orbitals (HOMO) at a certain distance from the surface. It is obvious that from the STM simulation that there is no one-to-one correspondence between regions of high local density of states and the atomic arrangement. Hence from the STM image alone it is rather difficult to deduce the molecular structure.

Often the organic overlayer structure studied in experiments[201] are still too large to be entirely treated using first-principles electronic structure codes. In order to still be able to address the structure and the properties of the organic layers from a theoretical and computation point of view, a hierarchical multiscale approach can be used. Force-field methods, i.e., empirical interaction potentials, often give a reliable description of the structure

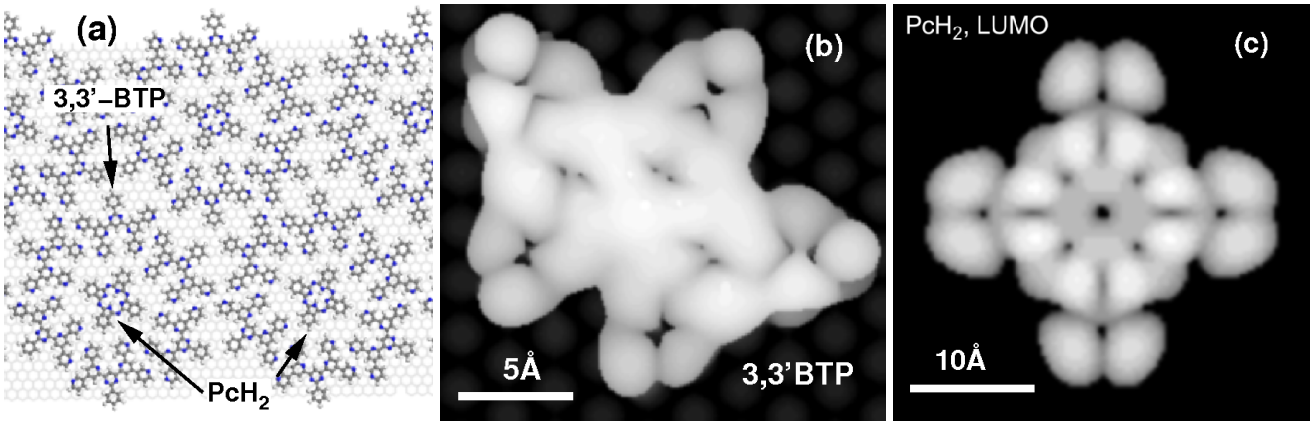

FIG. 26: Host-guest structure of a hexagonal oligopyridine network formed by 3,3'-BTP with phthalocyanine (PcH_2) embedded in the cavities of the network. (a) Structure of the network determined by force-field calculations; (b,c) STM simulation of the isolated building blocks of the host-guest structure, 3,3'-BTP and phthalocyanine, respectively, based on DFT calculations[200] (courtesy of D. Künzel).

of self-assemblied organic overlayers[202,203]. They can be used to determine the stable geometric structure of an organic layer. It should be noted that even if the evaluation of the total energy of an organic layer is still possible using DFT, force-field calculations can in any case be helpful. Usually the configuration space of possible adsorbate arrangements is immense, and the computationally inexpensive force-field methods can be used to do a pre-selection and pre-optimization of possible stable structures.

Nevertheless it is true that force-field calculations do not yield any information on the electronic structure so that no STM images can be derived from them. They can also not be used to determine any electronic, optical and catalytic functionality of an organic layer. Thus true electronic structure calculations are indispensable for a deeper analysis of the properties of organic layers. And if the first-principles treatment of whole structure of an organic layer is computationally too demanding, at least the building blocks of the structure might still be accessible by electronic structure calculations.

This approach is illustrated in Fig. 26. Oligopyridine molecules can form supramolecular structures on highly oriented pyrolytic graphite (HOPG)[201]. Figure 26 shows a hexagonal oligopyridine network consisting of bisterpyridine derivatives (3,3'-BTP) whose structure was calculated by force-field methods[200]. The open cavities of the oligopyridine network are filled with phthalocyanine (PcH_2) molecules. STM images of the isolated building blocks, 3,3'BTP and PcH_2, have been simulated based on DFT calculations. These organic assemblies are bound by weak hydrogen bonds which do not perturb the electronic structure of the molecules significantly. Hence the STM simulations of the isolated molecules should also be relevant for the interpretation of measured STM images of the whole network. Thus also the functionalization of the structure by embedding other molecules such as copper-phthalocyanine can be addressed.

This example demonstrates that DFT calculations together with force-field simulations allow the structure determination of organic monolayers on inorganic substrates. Still it should be mentioned that there is a dilemma in the first-principles treatment of these structures: DFT does not give an appropriate description of the van der Waals interaction which is often the dominant interaction for organic layers deposited on inorganic substrates[108]. High-quality quantum chemistry methods that correctly reproduce van der Waals forces are on the other hand computationally much too demanding. A possible way out of the dilemma consists of a hybrid QM/QM approach that has recently been proposed[110,111]. It uses the fact that the errors of exchange-correlations functionals are rather short-ranged. Hence many-body corrections for extended systems can be derived from quantum chemistry calculations on appropriately chosen finite representations, i.e., finite clusters.

6.2. Nanostructured organic junctions

The problem in the theoretical description of van der Waals forces does usually not arise in the theoretical description of SAMs formed by organic molecules with a sulfur endgroup since these molecules usually form strong bonds with metallic substrates such as Au(111). Recently it has been suggested that a sandwich structure formed by a SAM of 4-mercaptopyridine supported by Au(111) on which Pd is deposited could be used as a model system for a metal-molecule-metal contact[204]. Such structures could for example be the basis for molecular electronics devices.

Preliminary DFT calculations already suggested that the low density of states of the Pd layer on the SAM is due to the interaction between the Pd atoms and the nitrogen atom of the 4-mercaptopyridine[204]. Still, for a complete characterization it is necessary to identify the ex-

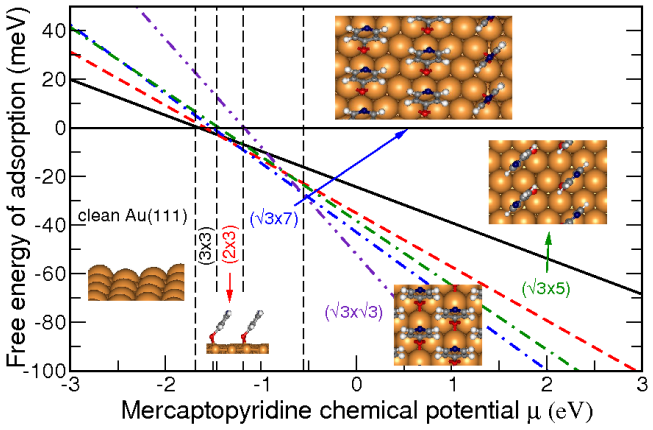

FIG. 27: Free surface energies of 4-mercaptopyridine on Au(111) as a function of the chemical potential[209]. The vertical dashed lines indicate the stability range of the different considered structures which are illustrated in the insets. The $(\sqrt{3} \times 5)$ structure (green dashed line) is not stable for any given value of μ according to the DFT calculations.

act structure of the metal-molecule-metal interfaces. The structure of mercaptopyridine SAMs on Au(111) in aqueous solution has already investigated intensively from an experimental point of view. Depending on the solution, different structures such a $(\sqrt{3} \times 5)$, $(\sqrt{3} \times 10)$[205] and $(\sqrt{3} \times 7)$[206] have been identified. This shows that the structure of the mercaptopyridine SAM can depend sensitively on the environment.

In order to model this dependence of the structure in thermal equilibrium with a reservoir, a thermodynamical concept recently applied to study the stability of surface oxides in heterogeneous catalysis at non-zero temperatures and pressures from first principles[207] can be used. This concept was already applied to the adsorption of acrolein on Pt(111) as a function of temperature and pressure[208]. It is based on the Gibbs free energy of adsorption $\Delta\gamma$ as a function of the temperature T and the pressure p[207],

$$\Delta\gamma(T,p) = \gamma(T,p,N_{\rm ads}) - \gamma_{\rm clean}(T,p,0) \quad (9)$$

$$= \frac{1}{A}\Delta G^{ads}(T,p) \quad (10)$$

$$= \frac{N_{\rm ads}}{A}\left(E_{\rm ads} - \mu_{\rm ads}(T,p)\right) \ , \quad (11)$$

where $N_{\rm ads}$ is the number of adsorbed molecules per surface unit cell area A, $\mu_{\rm ads}(T,p)$ is the chemical potential of the adsorbate, and $E_{\rm ads}$ is the adsorption energy which can for example be derived from *ab initio* total-energy calculations using Eq. (5). In the derivation of Eq. (11), entropic contributions to the free energy have been neglected since they are often rather small[207].

The free energy of adsorption $\Delta\gamma$ yields the stable adsorbate structure as a function of the chemical potential which itself is a function of temperature, pressure, concentration, etc. In Fig. 27, $\Delta\gamma$ is plotted for several mercaptopyridine structures on Au(111). The adsorption energy $E_{\rm ads}$ entering (11) was calculated for the mercaptopyridine radical. For a given chemical potential, the adsorbate structure with the lowest free energy should be the stable one in thermal equilibrium. Note that within this formalism environment-dependent free energies of adsorption can be evaluated without taking the environment explicitly into account.

Figure 27 shows that indeed the experimentally observed $(\sqrt{3} \times 7)$ structure[206] is thermodynamically stable in a certain range of the mercaptopyridine chemical potential. However, according to Fig. 27 the likewise observed $(\sqrt{3} \times 5)$ structure[205] should not be thermodynamically stable. Furthermore, for higher chemical potentials of mercaptopyridine a $(\sqrt{3}\times\sqrt{3})$ structure should be stable that had not been identified in experiments yet. There are several possible explanations for the discrepancies between theory and experiment. The DFT calculations might just not be accurate enough to yield the correct structures. Or the adsorbed mercaptopyridine radicals might form complexes with anions from the solution which would lead to an additional repulsion between the adsorbed molecules and would destabilize the high-density structures. Or it might well be that the observed structures do not correspond to equilibrium structures. Further theoretical and experimental investigations are obviously necessary, but free energy diagrams such as Fig. 27 will certainly serve as the basis for a fruitful collaboration between theory and experiment.

7. DYNAMICS OF THE ADSORPTION ON NANOSTRUCTURED SURFACES

7.1. Adsorption dynamics on precovered surfaces

In this review we already discussed that adsorbates can induce a nano-structuring of surfaces. Nowadays is has even become possible to perform *ab initio* molecular dynamics (AIMD) simulations of the adsorption dynamics on nanostructured surfaces in which the forces necessary to integrate the equations of motion are determined "on the fly" by first-principles calculations. While some years ago AIMD studies were restricted to a small number of trajectories[123,210], now a statistically meaningful number of AIMD trajectories can be determined, as a recent study of the H_2 dissociation on hydrogen-precovered Pd(111) and Pd(100) demonstrates[84].

This particular study was motivated by a STM study addressing the formation of ordered hydrogen layers on Pd(111)[211,212]. Surprisingly, they found that hydrogen molecules impinging on an almost complete hydrogen overlayer did not adsorb dissociatively in a hydrogen dimer vacancy. Rather, aggregates of three or more vacancies were required to dissociate hydrogen. These findings led to speculations that the accepted notion that two empty sites are required for the dissociative adsorption of diatomic molecules might not be correct[211,213].

However, a subsequent study based on density func-

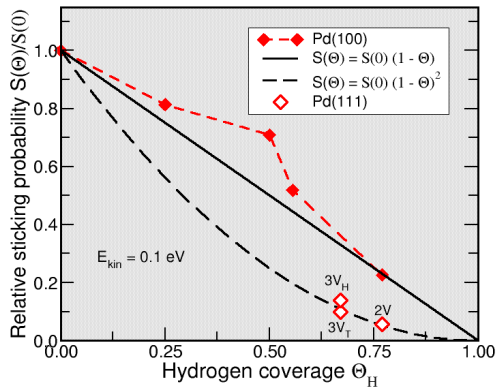

FIG. 28: Dissociative adsorption probability of hydrogen on hydrogen-covered Pd(100) and Pd(111) as a function of coverage for an initial kinetic energy of 0.1 eV. 2V, $3V_H$ and $3V_T$ denote the dimer vacancy and the trimer vacancy centered around a Pd hollow and a Pd top site, respectively (after [84]).

tional theory (DFT) showed that the dissociative adsorption of H_2 in a hydrogen dimer vacancy is still exothermic[214]. Still, the presence of the hydrogen overlayer has a poisoning effect; it leads to the formation of energetic barriers making the dissociative adsorption on hydrogen-precovered Pd(111) to an activated process.

These findings were confirmed in the AIMD study: at low initial kinetic energies of 0.02 eV no H_2 molecules were found to dissociate in a dimer vacancy within a (3×3) geometry corresponding to a surface coverage of $\Theta_H = 7/9 \approx 0.78$[84]. This result also provides an explanation for the experimental results. At the low temperatures of 70 K used in the experiment[211] the H_2 molecules were just too slow to cross the dissociation barrier.

At higher kinetic energies, however, H_2 molecules can adsorb dissociatively in a dimer vacancy on hydrogen-covered Pd(111). This is shown in Fig. 28 where the sticking probabilities for both Pd(111) and Pd(100) are plotted as a function of the hydrogen coverage normalized to the value at the corresponding clean Pd surfaces for an kinetic energy of 0.1 eV. The sticking probabilities were determined by averaging over at least 200 trajectories for each coverage leading to a statistical error of $\sqrt{s(1-s)}/\sqrt{200} \leq 0.035$, where s is the adsorption probability. The trajectories were started 4 Å above the surface with random initial lateral positions and molecular orientations. The classical equations of motion were integrated using the Verlet algorithm with a time step of 1 fs within the microcanonical ensemble. On Pd(111), a small, but non-vanishing relative adsorption probability of 0.05 is found in the dimer vacancy (2V). At the trimer vacancies on Pd(111) centered either around a hollow site ($3V_H$) or a Pd top site ($3V_T$), the adsorption probability is at least twice as large as on the dimer vacancy (2V). Since the area of the trimer vacancy is only larger by 50% compared to the dimer vacancy, this indicates that it is not only the area of the vacancies that determines the adsorption probability.

The same is true for the adsorption on the hydrogen-precovered Pd(100) surface. In Fig. 28, two curves corresponding to $S(\Theta_H) = S(0)(1-\Theta_H)$ and $S(\Theta_H) = S(0)(1-\Theta_H)^2$ are included which would correspond to the sticking probability if it was determined by pure site-blocking requiring one or two empty sites, respectively. At low and intermediate coverages the sticking probability of H_2 at Pd(100) is significantly larger than predicted from a simple site-blocking picture, in particular for $\Theta_H = 0.5$. Running additional AIMD trajectories with the substrate kept fixed show that it is the energy transfer from the impinging H_2 molecule to the substrate and the rearrangement of the substrate atoms that leads to this enhanced sticking probability compared to pure site blocking, in spite of the fact that the hydrogen coverage leads to a small poisoning effect which should reduce the sticking probability[84].

The AIMD simulations do not only yield statistically reliable sticking probabilities, they also allow for valuable microscopic insights into the dissociative adsorption dynamics. In Fig. 29, snapshots of three typical adsorption events at the $H(3\times 3)$/Pd(100) surface with a dimer vacancy are shown. A dissociative adsorption event is illustrated in Figs. 29a and b. The H_2 molecule first hits the Pd surface close to a Pd top site. In fact, before dissociating the H_2 molecule becomes dynamically trapped[215–217]: the molecule does not directly find the pathway towards dissociation. However, it starts rotating, vibrating and moving laterally, and due the conversion of the initial kinetic energy into internal and lateral degrees of freedom, the H_2 molecule can not escape back into the gas phase. But after about 1 ps, the molecule dissociates (see Fig. 29a for the configuration just before dissociation). Upon dissociation, the molecules gains almost 1 eV of kinetic energy which is then first transfered to the hydrogen overlayer. There is a strong energy transfer to the hydrogen overlayer which results in large vibrational amplitudes of the hydrogen atoms. This is visible as the large displacements of the hydrogen atoms from their equilibrium sites which in Fig. 29b is particularly pronounced for the hydrogen atoms at the left of the original vacancy site.

At the hydrogen-covered Pd(100) surface, the impinging H_2 molecules do not necessarily either dissociatively adsorb or scatter back into the gas phase. In fact, there exists a molecular precursor state above the top sites which becomes stabilized due to the poisoning effects of the pre-adsorbed hydrogen atoms, very similar to the one already identified at the hydrogen-covered stepped Pd(210) surface[45,47] (see Fig. 8). This state also corresponds to a PdH_2 complex with the H_2 molecule moving relatively freely around the ontop position. About 5% of the impinging H_2 molecules become trapped in these sites. Figures 29c and d show a top and a side view of a H_2 molecule trapped in such a molecular precursor. This state has not been identified experimentally yet, however, it should be detectable at low surface temperatures by,

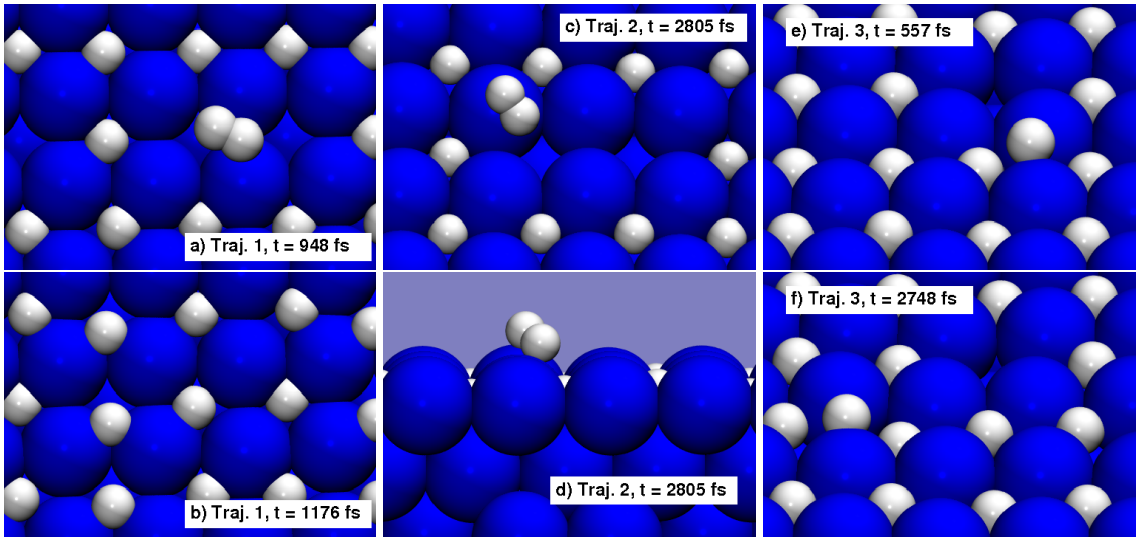

FIG. 29: Snapshots of three trajectories calculated in *ab initio* molecular dynamics simulations[84] within a (3×3) surface periodicity illustrating details of the adsorption dynamics at a hydrogen-covered Pd(100) surface with a dimer vacancy.

e.g., isotope exchange experiments since it is bound by 0.1 eV.

Another interesting adsorption geometry that has not been discussed before is shown Figs. 29e and f. One of the impinging hydrogen atom enters a four-fold hollow site adjacent to an occupied site while the other one remains trapped at the bridge site (Fig. 29e). The additional bridge-site hydrogen atom can actually move in an exchange mechanism[218]: it replaces one of the adsorbed hydrogen atoms at the four-fold hollow sites which is then pushed up to an adjacent bridge site. As Fig. 29f demonstrates, after 2 ps there have been two exchange events so that there is a bridge-site hydrogen atom two lattice sites away from the original site. This diffusion will end when the exchanged hydrogen atom finds an empty stable four-fold hollow site.

8. CONCLUSIONS AND OUTLOOK

In this review, theoretical studies of the adsorption of atoms and molecules at nanostructured surfaces using first-principles electronic structure methods have been discussed. Such studies have only become possible in the last ten years because of the increase in computer power and the development of more efficient algorithms. Due to the fact that these first-principles calculations also yield information on the electronic structure underlying the bond-making and bond-breaking process, fundamental concepts about the specific chemical and catalytical properties of nanostructured surfaces have been derived.

However, it is fair to say that the size of the nanostructures treated in these studies is still limited. Whereas many nanostructures studied by experimentalists contain several thousands of atoms, computational studies are often restricted to only hundreds of atoms. It will probably take some time before supported clusters with thousands of atoms can be handled by *ab initio* total-energy calculations. However, it is questionable whether large-scale *ab initio* total-energy calculations are really necessary for a deeper understanding of nanostructured surfaces. The more complex a system is, the harder it is to analyze its basic properties and to derive general principles. The important role of special sites and configurations of nanostructures, e.g., can already be investigated using smaller systems, as illustrated in this review, and other aspects of the nanostructures might be treated by more efficient, approximate methods such as multi-scale methods.

In spite of the technical obstacles, there will certainly be a growing number of first-principles studies addressing the adsorption on nanostructured surfaces since the interest in nanostructured surfaces and their technological applications will still increase. Although there is also significant progress in the experimental techniques, theoretical studies will remain to be an indispensable tool for the interpretation and analysis of structures and processes on the nano-scale. We will even see closer and closer collaborations between theory and experiment in the future. The theoretical investigation of adsorption on nanostructured surfaces is certainly a challenging and demanding research field, but at the same time it is an exciting and rewarding area that will prosper in the years to come.

Acknowledgments

It is a pleasure to acknowledge all the co-workers and friends who have helped me to gain insight into the subject covered in this review. These are in particular Jürgen Behm, Wilhelm Brenig, Andreas Eichler, Jürgen Hafner, Peter Jakob, Bjørk Hammer, Wolfgang Heckl, Ulrich

Höfer, Harry Hoster, Dieter Kolb, Peter Kratzer, Georg Kresse, Horia Metiu, Eckhard Pehlke, Karsten Reuter, Philippe Sautet, Matthias Scheffler, Ulrich Ziener, and many others who hopefully do not feel offended by not being mentioned. Furthermore, my own research on the adsorption on nanostructured surfaces would not have been possible without the talented students and PostDocs in my my research groups at the Technical University of Munich and the University of Ulm including Arezoo Dianat, Yoshihiro Gohda, Jan Kucera, Daniela Künzel, Markus Lischka, Thomas Markert, Christian Mosch, Ata Roudgar, Sung Sakong, and Katrin Tonigold. This work was supported in part by the Deutsche Forschungsgemeinschaft (DFG) within the collaborative research center SFB 569, the priority programmes SPP 1030 and SPP 1091, and DFG contract GR 1503/11-1.

[1] G. Binnig, H. Rohrer, C. Gerber, and E. Weibel, Phys. Rev. Lett. **49**, 57 (1982).
[2] C. B. Duke and E. W. Plummer, eds., *Frontiers in Surface and Interface Science* (North-Holland, Amsterdam, 2002).
[3] A. Groß, Surf. Sci. **500**, 347 (2002).
[4] C. Stampfl, M. V. Ganduglia-Pirovano, K. Reuter, and M. Scheffler, Surf. Sci. **500**, 368 (2002).
[5] B. Hammer, Topics Catal. **37**, 3 (2006).
[6] C. R. Henry, Surf. Sci. Rep. **31**, 235 (1998).
[7] K. H. Hansen, S. Stempel, E. Lægsgaard, M. Bäumer, and H.-J. Freund, Phys. Rev. Lett. **83**, 4120 (1999).
[8] H.-J. Freund, Surf. Sci. **500**, 271 (2002).
[9] A. T. Bell, Science **299**, 1688 (2003).
[10] A. Sanchez, S. Abbet, U. Heiz, W.-D. Schneider, H. Häkkinen, R. N. Barnett, and U. Landman, J. Phys. Chem. A **103**, 9573 (1999).
[11] P. Hohenberg and W. Kohn, Phys. Rev. **136**, B864 (1964).
[12] W. Kohn and L. Sham, Phys. Rev. **140**, A1133 (1965).
[13] W. Kohn, Rev. Mod. Phys. **71**, 1253 (1999).
[14] R. M. Dreizler and E. K. U. Gross, *Density Functional Theory: An Approach to the Quantum Many-Body Problem* (Springer, Berlin, 1990).
[15] A. Groß, *Theoretical surface science – A microscopic perspective* (Springer, Berlin, 2002).
[16] A. Szabo and N. S. Ostlund, *Modern quantum chemistry: introduction to advanced electronic structure theory* (McGraw-Hill, New York, 1989).
[17] K. Raghavachari and J. Anderson, J. Phys. Chem. **100**, 12960 (1996).
[18] J. A. Pople, Rev. Mod. Phys. **71**, 1267 (1999).
[19] B. J. Zhou, V. L. Ligneres, and E. A. Carter, J. Chem. Phys. **122**, 044103 (2005).
[20] B. Hammer, M. Scheffler, K. Jacobsen, and J. Nørskov, Phys. Rev. Lett. **73**, 1400 (1994).
[21] B. G. Johnson, P. M. W. Gill, and J. A. Pople, J. Chem. Phys. **98**, 5612 (1993).
[22] A. D. Becke, Phys. Rev. A **38**, 3098 (1988).
[23] J. P. Perdew, K. Burke, and M. Ernzerhof, Phys. Rev. Lett. **77**, 3865 (1996).
[24] B. Hammer, L. B. Hansen, and J. K. Nørskov, Phys. Rev. B **59**, 7413 (1999).
[25] J. L. Whitten and H. Yang, Surf. Sci. Rep. **24**, 55 (1996).
[26] M. Fuchs and M. Scheffler, Comput. Phys. Commun. **119**, 67 (1999).
[27] D. Vanderbilt, Phys. Rev. B **41**, 7892 (1990).
[28] P. E. Blöchl, Phys. Rev. B **50**, 17953 (1994).
[29] G. Kresse and D. Joubert, Phys. Rev. B **59**, 1758 (1999).
[30] G. Kresse and J. Furthmüller, Phys. Rev. B **54**, 11169 (1996).
[31] M. Bockstedte, A. Kley, J. Neugebauer, and M. Scheffler, Comput. Phys. Commun. **107**, 187 (1997).
[32] B. Hammer, L. B. Hansen, and J. K. Nørskov, Phys. Rev. B **59**, 7413 (1999).
[33] A. Bogicevic, S. Ovesson, P. Hyldgaard, B. I. Lundqvist, H. Brune, and D. R. Jennison, Phys. Rev. Lett. **85**, 1910 (2000).
[34] B. Hammer and J. K. Nørskov, Surf. Sci. **343**, 211 (1995).
[35] B. Hammer and J. K. Nørskov, Nature **376**, 238 (1995).
[36] K. Fukui, Science **218**, 747 (1982).
[37] R. Hoffmann, Rev. Mod. Phys. **60**, 601 (1988).
[38] B. Hammer, O. H. Nielsen, and J. K. Nørskov, Catal. Lett. **46**, 31 (1997).
[39] V. Pallassana, M. Neurock, L. B. Hansen, B. Hammer, and J. K. Nørskov, Phys. Rev. B **60**, 6146 (1999).
[40] A. Ruban, B. Hammer, P. Stoltze, H. L. Skriver, and J. K. Nørskov, J. Mol. Catal. A **115**, 421 (1997).
[41] M. Mavrikakis, B. Hammer, and J. K. Nørskov, Phys. Rev. Lett. **81**, 2819 (1998).
[42] A. Roudgar and A. Groß, Phys. Rev. B **67**, 033409 (2003).
[43] A. Roudgar and A. Groß, J. Electroanal. Chem. **548**, 121 (2003).
[44] A. Groß, Topics Catal. **37**, 29 (2006).
[45] M. Lischka and A. Groß, Phys. Rev. B **65**, 075420 (2002).
[46] N. W. Ashcroft and N. D. Mermin, *Solid State Physics* (Saunders College, Philadelphia, 1976).
[47] P. K. Schmidt, K. Christmann, G. Kresse, J. Hafner, M. Lischka, and A. Groß, Phys. Rev. Lett. **87**, 096103 (2001).
[48] B. Lang, R. W. Joyner, and G. A. Somorjai, Surf. Sci **30**, 440 (1972).
[49] R. Q. Hwang, J. Schröder, C. Günther, and R. J. Behm, Phys. Rev. Lett. **67**, 3279 (1991).
[50] P. Gambardella, Ž. Šljivančanin, B. Hammer, M. Blanc, K. Kuhnke, and K. Kern, Phys. Rev. Lett. **87**, 056103 (2001).
[51] A. C. Luntz, M. D. Williams, and D. S. Bethune, J. Chem. Phys. **89**, 4381 (1988).
[52] W. Wurth, J. Stöhr, P. Feulner, X. Pan, K. R. Bauchspiess, Y. Baba, E. Hudel, G. Rocker, and D. Menzel, Phys. Rev. Lett. **65**, 2426 (1990).
[53] C. T. Rettner and C. B. Mullins, J. Chem. Phys. **94**, 1626 (1991).
[54] J. Wintterlin, R. Schuster, and G. Ertl, Phys. Rev. Lett. **77**, 123 (1996).
[55] B. C. Stipe, M. A. Rezaei, W. Ho, S. Gao, M. Persson, and B. I. Lundqvist, Phys. Rev. Lett. **78**, 4410 (1997).
[56] P. D. Nolan, B. R. Lutz, P. L. Tanaka, J. E. Davis, and C. B. Mullins, J. Chem. Phys. **111**, 3696 (1999).
[57] A. Eichler and J. Hafner, Phys. Rev. Lett. **79**, 4481 (1997).
[58] A. Eichler, F. Mittendorfer, and J. Hafner, Phys. Rev. B

62, 4744 (2000).
[59] A. Groß, A. Eichler, J. Hafner, M. J. Mehl, and D. A. Papaconstantopoulos, Surf. Sci. **539**, L542 (2003).
[60] A. Groß, A. Eichler, J. Hafner, M. J. Mehl, and D. A. Papaconstantopoulos, J. Chem. Phys. **124**, 174713 (2006).
[61] C. Sendner and A. Groß, J. Chem. Phys. **127**, 014704 (2007).
[62] Ž. Šljivančanin and B. Hammer, Surf. Sci. **515**, 235 (2002).
[63] P. J. Feibelman, S. Esch, and T. Michely, Phys. Rev. Lett. **77**, 2257 (1996).
[64] S. Dahl, A. Logadottir, R. C. Egeberg, J. H. Larsen, I. Chorkendorff, E. Törnqvist, and J. K. Nørskov, Phys. Rev. Lett. **83**, 1814 (1999).
[65] S. Dahl, E. Törnqvist, and I. Chorkendorff, J. Catal. **192**, 381 (2000).
[66] K. Jacobi, H. Dietrich, and G. Ertl, Appl. Surf. Sci. **121/122**, 558 (1997).
[67] S. Dahl, P. A. Taylor, E. Törnqvist, and I. Chorkendorff, J. Catal. **178**, 679 (1998).
[68] A. Logadottir and J. K. Nørskov, J. Catal. **220**, 273 (2003).
[69] J. J. Mortensen, B. Hammer, and J. Nørskov, Phys. Rev. Lett. **80**, 4333 (1998).
[70] B. Hammer, Phys. Rev. Lett **83**, 3681 (1999).
[71] T. Zambelli, J. Wintterlin, J. Trost, and G. Ertl, Science **273**, 1688 (1996).
[72] K. Christmann, Surf. Sci. Rep. **9**, 1 (1988).
[73] A.-S. Mårtensson, C. Nyberg, and S. Andersson, Phys. Rev. Lett. **57**, 2045 (1986).
[74] K. Svensson, L. Bengtsson, J. Bellman, M. Hassel, M. Persson, and S. Andersson, Phys. Rev. Lett. **83**, 124 (1999).
[75] L. Bengtsson, K. Svensson, M. Hassel, J. Bellman, M. Persson, and S. Andersson, Phys. Rev. B **61**, 16921 (2000).
[76] A. Groß, Appl. Phys. A **67**, 627 (1998).
[77] M. Lischka and A. Groß, in *Recent Developments in Vacuum Science and Technology*, edited by J. Dabrowski (Research Signpost, Kerala (India), 2003), pp. 111–132.
[78] G.-J. Kroes, A. Groß, E. J. Baerends, M. Scheffler, and D. A. McCormack, Acc. Chem. Res. **35**, 193 (2002).
[79] S. Wilke and M. Scheffler, Phys. Rev. B **53**, 4926 (1996).
[80] W. Dong and J. Hafner, Phys. Rev. B **56**, 15396 (1997).
[81] V. Ledentu, W. Dong, and P. Sautet, Surf. Sci. **412**, 518 (1998).
[82] X.-G. Zhang, M. A. Van Hove, G. A. Somorjai, P. J. Rous, D. Tobin, A. Gonis, J. M. MacLaren, K. Heinz, M. Michl, H. Lindner, et al., Phys. Rev. Lett. **67**, 1298 (1991).
[83] A. Dedieu, Chem. Rev. **100**, 543 (2000).
[84] A. Groß and A. Dianat, Phys. Rev. Lett. **98**, 206107 (2007).
[85] R. F. Service, Science **305**, 958 (2004).
[86] M. Lischka, C. Mosch, and A. Groß, Surf. Sci. **570**, 227 (2004).
[87] R. J. Behm, K. Christmann, G. Ertl, and M. A. Van Hove, J. Chem. Phys. **73**, 2984 (1980).
[88] A. Eichler and J. Hafner, Phys. Rev. B **57**, 10110 (1998).
[89] P. Hu, D. A. King, M.-H. Lee, and M. C. Payne, Chem. Phys. Lett. **246**, 73 (1995).
[90] M. Kittel, R. Terborg, M. Polcik, A. M. Bradshaw, R. L. Toomes, D. P. Woodruff, and E. Rotenberg, Surf. Sci. **511**, 34 (2002).
[91] H. S. Kato, H. Okuyama, J. Yoshinubo, and M. Kawai, Surf. Sci. **513**, 239 (2002).
[92] T. E. Madey, J. T. Yates, Jr., A. M. Bradshaw, and F. M. Hoffmann, Surf. Sci. **89**, 370 (1979).
[93] H. Conrad, G. Ertl, J. Koch, and E. E. Latta, Surf. Sci. **43**, 462 (1974).
[94] P. K. Schmidt, Ph.D. thesis, Freie Universität Berlin (2002).
[95] E. Christoffersen, P. Stoltze, and J. K. Nørskov, Surf. Sci. **505**, 200 (2002).
[96] L. Savio, L. Vattuone, and M. Rocca, Phys. Rev. Lett. **87**, 276101 (2001).
[97] L. Savio, L. Vattuone, and M. Rocca, J. Phys.: Condens. Matter **14**, 6065 (2002).
[98] L. Vattuone, L. Savio, and M. Rocca, Phys. Rev. Lett. **90**, 228302 (2003).
[99] N. Bonini, A. Kokalj, A. Dal Corso, S. de Gironcoli, and S. Baroni, Phys. Rev. B **69**, 195401 (2004).
[100] A. Kokalj, N. Bonini, A. Dal Corso, S. de Gironcoli, and S. Baroni, Surf. Sci. **566**, 1107 (2004).
[101] N. Bonini, A. Dal Corso, A. Kokalj, S. de Gironcoli, and S. Baroni, Surf. Sci. **587**, 50 (2005).
[102] T. Schimizu and M. Tsukada, Surf. Sci. **295**, L1017 (1993).
[103] D. J. Coulman, J. Wintterlin, R. J. Behm, and G. Ertl, Phys. Rev. Lett. **64**, 1761 (1990).
[104] S. Sakong and A. Groß, J. Phys. Chem. A **111**, 8814 (2007).
[105] L. Delle Site and D. Sebastiani, Phys. Rev. B **70**, 115401 (2004).
[106] R. T. Vang, K. Honkala, S. Dahl, E. K. Vestergaard, J. Schnadt, E. Lægsgaard, J. K. Clausen, B. S. Nørskov, and F. Besenbacher, Surf. Sci. **600**, 66 (2006).
[107] J. M. Thomas and W. J. Thomas, *Principles and Practice of Heterogeneous Catalysis* (VCH-Wiley, Weinheim, 1997).
[108] F. Ortmann, W. G. Schmidt, and F. Bechstedt, Phys. Rev. Lett. **95**, 186101 (2005).
[109] C. Tuma and J. Sauer, Chem. Phys. Lett. **387**, 388 (2004).
[110] C. Tuma and J. Sauer, Phys. Chem. Chem. Phys. **8**, 3955 (2006).
[111] Q.-M. Hu and K. R. M. Scheffler, Phys. Rev. Lett. **98**, 176103 (2007).
[112] R. T. Vang, K. Honkala, S. Dahl, E. K. Vestergaard, J. Schnadt, E. Lægsgaard, J. K. Clausen, B. S. Nørskov, and F. Besenbacher, Nat. Mater. **4**, 160 (2005).
[113] Ž. Šljivančanin, K. V. Gothelf, and B. Hammer, J. Am. Chem. Soc. **124**, 14789 (2002).
[114] A. Kokalj, A. Dal Corso, S. de Gironcoli, and S. Baroni, J. Phys. Chem. B **106**, 9839 (2002).
[115] A. Kokalj, A. Dal Corso, S. de Gironcoli, and S. Baroni, Surf. Sci. **566**, 1018 (2004).
[116] C. F. McFadden, P. S. Cremer, and A. J. Gellman, Langmuir **12**, 2483 (1996).
[117] G. A. Attard, J. Phys. Chem. B **105**, 3158 (2001).
[118] C. D. Bain, J. Evall, and G. M. Whitesides, J. Am. Chem. Soc. **111**, 7155 (1989).
[119] A. Kühnle, T. R. Linderoth, B. Hammer, and F. Besenbacher, Nature **415**, 891 (2002).
[120] T. D. Booth, D. Wahnon, and I. Wainer, Chirality **9**, 96 (1997).
[121] G. S. Higashi, Y. J. Chabal, G. W. Trucks, and K. Raghavachari, Appl. Phys. Lett. **56**, 656 (1990).

[122] E. Pehlke and M. Scheffler, Phys. Rev. Lett. **74**, 952 (1995).
[123] A. Groß, M. Bockstedte, and M. Scheffler, Phys. Rev. Lett. **79**, 701 (1997).
[124] C. Filippi, S. B. Healy, P. Kratzer, E. Pehlke, and M. Scheffler, Phys. Rev. Lett. **89**, 166102 (2002).
[125] W. Brenig, A. Groß, and R. Russ, Z. Phys. B **96**, 231 (1994).
[126] W. Brenig and M. F. Hilf, J. Phys. Condens. Mat. **13**, R61 (2001).
[127] P. Kratzer, E. Pehlke, M. Scheffler, M. B. Raschke, and U. Höfer, Phys. Rev. Lett. **81**, 5596 (1998).
[128] E. Pehlke and J. Tersoff, Phys. Rev. Lett. **67**, 1290 (1991).
[129] P. Krüger and J. Pollmann, Phys. Rev. Lett. **74**, 1155 (1995).
[130] M. Rohlfing, P. Krüger, and J. Pollmann, Phys. Rev. B **52**, 1905 (1995).
[131] E. Pehlke and P. Kratzer, Phys. Rev. B **59**, 2790 (1999).
[132] A. Biedermann, E. Knoesel, Z. Hu, and T. F. Heinz, Phys. Rev. Lett. **83**, 1810 (1999).
[133] M. Dürr, Z. Hu, A. Biedermann, U. Höfer, and T. F. Heinz, Phys. Rev. Lett. **88**, 046104 (2002).
[134] E. Pehlke, Phys. Rev. B **62**, 12932 (2000).
[135] K. W. Kolasinski, W. Nessler, K.-H. Bornscheuer, and E. Hasselbrink, J. Chem. Phys. **101**, 7082 (1994).
[136] P. Bratu, K. L. Kompa, and U. Höfer, Chem. Phys. Lett. **251**, 1 (1996).
[137] K. W. Kolasinski, W. Nessler, A. de Meijere, and E. Hasselbrink, Phys. Rev. Lett. **72**, 1356 (1994).
[138] U. Landman and W. D. Luedtke, Faraday Diss. **125**, 1 (2004).
[139] S. J. Tauster, S. C. Fung, and R. L. Garten, J. Am. Chem. Soc. **100**, 170 (1978).
[140] D. R. Jennison, O. Dulub, W. Hebenstreit, and U. Diebold, Surf. Sci. **106**, L677 (2001).
[141] M. Valden, X. Lai, and D. W. Goodman, Science **281**, 1647 (1998).
[142] M. Haruta, Catal. Today **36**, 153 (1997).
[143] P. Pyykko, Angew. Chemie, Int. Ed. **43**, 4412 (2004).
[144] G. Mills, M. S. Gordon, and H. Metiu, J. Chem. Phys. **118**, 4198 (2003).
[145] S. A. Varganov, R. M. Olson, M. S. Gordon, and H. Metiu, J. Chem. Phys. **119**, 2531 (2003).
[146] M. Mavrikakis, P. Stoltz, and J. K. Nørskov, Catal. Lett. **64**, 101 (2000).
[147] N. Lopez and J. K. Nørskov, J. Am. Chem. Soc. **124**, 11262 (2002).
[148] N. Lopez, T. V. W. Janssens, B. S. Clausen, Y. Xu, M. Mavrikakis, T. Bligaard, and J. K. Nørskov, J. Catal. **223**, 232 (2004).
[149] L. Piccolo, D. Loffreda, F. J. C. S. Aires, C. Deranlot, Y. Jugnet, P. Sautet, and J. C. Bertolini, Surf. Sci. **566**, 995 (2004).
[150] J. P. Perdew, J. A. Chevary, S. H. Vosko, K. A. Jackson, M. R. Pederson, D. J. Singh, and C. Fiolhais, Phys. Rev. B **46**, 6671 (1992).
[151] Z.-P. Liu, P. Hu, and A. Alavi, J. Am. Chem. Soc. **124**, 11262 (2002).
[152] Y. Wang and G. S. Hwang, Surf. Sci. **542**, 72 (2003).
[153] A. Vittadini and A. Selloni, J. Chem. Phys. **117**, 353 (2002).
[154] N. Lopez, J. K. Nørskov, T. V. W. Janssens, A. Carlsson, A. Puig-Molina, B. S. Clausen, and J. D. Grunwaldt, J. Catal. **225**, 86 (2004).
[155] L. M. Molina and B. Hammer, Phys. Rev. Lett. **90**, 206102 (2003).
[156] L. M. Molina, M. D. Rasmussen, and B. Hammer, J. Chem. Phys. **120**, 7673 (2004).
[157] D. Matthey, J. G. Wang, S. Wendt, J. Matthiesen, R. Schaub, E. Lægsgaard, B. Hammer, and F. Besenbacher, Science **315**, 1692 (2007).
[158] L. M. Molina and B. Hammer, Phys. Rev. B **69**, 155424 (2004).
[159] M. D. Rasmussen, L. M. Molina, and B. Hammer, J. Chem. Phys. **120**, 988 (2004).
[160] M. S. Chen and D. W. Goodman, Science **306**, 252 (2004).
[161] B. Yoon, H. Häkkinen, U. Landman, A. S. Wörz, J.-M. Antonietti, S. Abbet, and U. Heiz, Science **307**, 403 (2005).
[162] S. Abbet, U. Heiz, A. M. Ferrari, L. Giordano, C. Di Valentin, and G. Pacchioni, Thin Solid Films **400**, 37 (2001).
[163] H. Häkkinen, S. Abbet, A. Sanchez, U. Heiz, and U. Landman, Angew. Chem. Int. Ed. **42**, 1297 (2003).
[164] P. M. Ajayan and L. D. Marks, Nature **338**, 139 (1989).
[165] D. Ricci, A. Bongiorno, G. Pacchioni, and U. Landman, Phys. Rev. Lett. **97**, 036106 (2006).
[166] M. Sterrer, T. Risse, M. Heyde, H.-P. Rust, and H.-J. Freund, Phys. Rev. Lett. **98**, 206103 (2007).
[167] D. M. Kolb, Surf. Sci. **500**, 722 (2002).
[168] D. M. Kolb, R. Ullmann, and T. Will, Science **275**, 1097 (1997).
[169] G. E. Engelmann, J. C. Ziegler, and D. M. Kolb, J. Electrochem. Soc. **145**, L33 (1998).
[170] A. Roudgar and A. Groß, Surf. Sci. **559**, L180 (2004).
[171] W. Dong, V. Ledentu, P. Sautet, A. Eichler, and J. Hafner, Surf. Sci. **411**, 123 (1998).
[172] D. M. Kolb, G. E. Engelmann, and J. C. Ziegler, Angew. Chemie, Int. Ed. **39**, 1123 (2000).
[173] M. G. Del Popolo, E. P. M. Leiva, H. Kleine, J. Meier, U. Stimming, M. Mariscal, and W. Schmickler, Appl. Phys. Lett. **81**, 2635 (2002).
[174] M. G. Del Popolo, E. P. M. Leiva, H. Kleine, J. Meier, U. Stimming, M. Mariscal, and W. Schmickler, Electrochim. Acta **48**, 1287 (2003).
[175] S. M. Foiles, M. I. Baskes, and M. S. Daw, Phys. Rev. B **33**, 7983 (1986).
[176] M. S. Daw, S. M. Foiles, and M. I. Baskes, Mater. Sci. Rep. **9**, 252 (1993).
[177] M. G. Del Popolo, E. P. M. Leiva, M. Mariscal, and W. Schmickler, Nanotechnology **14**, 1009 (2003).
[178] A. Roudgar, private communication.
[179] J. A. Rodriguez, Surf. Sci. Rep. **24**, 223 (1996).
[180] J. H. Sinfelt, Surf. Sci. **500**, 923 (2002).
[181] J. Greeley and M. Mavrikakis, Nature Materials **3**, 810 (2004).
[182] Y. Gohda and A. Groß, J. Electroanal. Chem. **607**, 47 (2007).
[183] A. Bergbreiter, H. E. Hoster, S. Sakong, A. Groß, and R. J. Behm, Phys. Chem. Chem. Phys. **9**, 5127 (2007).
[184] S. Müller, J. Phys.: Cond. Matter **15**, R1429 (2003).
[185] W. H. M. Sachtler, Faraday Diss. **72**, 7 (1981).
[186] S. Sakong, C. Mosch, and A. Groß, Phys. Chem. Chem. Phys. **9**, 2216 (2007).
[187] M. T. M. Koper, T. E. Shubina, and R. A. van Santen, J. Phys. Chem. B **106**, 686 (2002).
[188] T. E. Shubina and M. T. M. Koper, Electrochim. Acta **47**, 3621 (2002).

[189] A. Schlapka, M. Lischka, A. Groß, U. Käsberger, and P. Jakob, Phys. Rev. Lett. **91**, 016101 (2003).
[190] M. Lischka, C. Mosch, and A. Groß, Electrochim. Acta **52**, 2219 (2007).
[191] Y. Gohda and A. Groß, Surf. Sci. **601**, 3702 (2007).
[192] O. R. Inderwildi, S. J. Jenkins, and D. A. King, Surf. Sci. **601**, L103 (2007).
[193] F. Rosei, M. Schunack, Y. Naitoh, P. Jiang, A. Gourdon, E. Lægsgaard, I. Stensgaard, C. Joachim, and F. Besenbacher, Prog. Surf. Sci. **71**, 95 (2003).
[194] S. J. Sowerby, W. M. Heckl, and G. B. Petersen, J. Mol. Evol. **43**, 419 (1996).
[195] W. M. Heckl, in *Astrobiology, The Quest for the Conditions of Life*, edited by G. Horneck and C. Baumstark-Khan (Springer, Berlin, 2002).
[196] D. Tománek, S. G. Louie, H. J. Mamin, D. W. Abraham, R. E. Thomson, E. Ganz, and J. Clark, Phys. Rev. B **35**, 7790 (1987).
[197] J. Tersoff and D. R. Hamann, Phys. Rev. Lett. **50**, 1998 (1983).
[198] W. A. Hofer, A. S. Foster, and A. Shluger, Rev. Mod. Phys. **75**, 1287 (2003).
[199] J. Freund, M. Edelwirth, P. Kröbel, and W. M. Heckl, Phys. Rev. B **55**, 5394 (1997).
[200] D. Künzel and A. Groß, in preparation.
[201] C. Meier, U. Ziener, K. Landfester, and P. Weihrich, J. Phys. Chem. B **109**, 21015 (2005).
[202] M. Edelwirth, J. E. Freund, S. J. Sowerby, and W. M. Heckl, Surf. Sci. **417**, 201 (1998).
[203] K. Shinoda, W. Shinoda, C. C. Liew, S. Tsuzuki, Y. Morikawa, and M. Mikami, Surf. Sci. **556**, 109 (2004).
[204] H.-G. Boyen, P. Ziemann, U. Wiedwald, V. Ivanova, D. M. Kolb, S. Sakong, A. Groß, A. Romanyuk, M. Büttner, and P. Oelhafen, Nature Mater. **5**, 394 (2006).
[205] T. Baunach, V. Ivanova, D. A. Scherson, and D. M. Kolb, Langmuir **20**, 2797 (2004).
[206] W. Zhou, T. Baunach, V. Ivanova, and D. M. Kolb, Langmuir **20**, 4590 (2004).
[207] K. Reuter and M. Scheffler, Phys. Rev. B **65**, 035406 (2001).
[208] D. Loffreda, F. Delbecq, and P. Sautet, Chem. Phys. Lett. **405**, 434 (2005).
[209] J. Kucera and A. Groß, in preparation.
[210] L. C. Ciacchi and M. C. Payne, Phys. Rev. Lett. **92**, 176104 (2004).
[211] T. Mitsui, M. K. Rose, E. Fomin, D. F. Ogletree, and M. Salmeron, Nature **422**, 705 (2003).
[212] T. Mitsui, M. K. Rose, E. Fomin, D. F. Ogletree, and M. Salmeron, Surf. Sci. **540**, 5 (2003).
[213] M. Salmeron, Topics Catal. **36**, 55 (2005).
[214] N. Lopez, Z. Lodziana, F. Illas, and M. Salmeron, Phys. Rev. Lett. **93**, 146103 (2004).
[215] A. Groß and M. Scheffler, J. Vac. Sci. Technol. A **15**, 1624 (1997).
[216] C. Crespos, H. F. Busnengo, W. Dong, and A. Salin, J. Chem. Phys. **114**, 10954 (2001).
[217] H. F. Busnengo, W. Dong, and A. Salin, Chem. Phys. Lett. **320**, 328 (2000).
[218] P. J. Feibelman, Phys. Rev. Lett. **65**, 729 (1990).